A PLANETARY-SCALE DISTURBANCE IN A LONG LIVING THREE VORTEX COUPLED SYSTEM IN SATURN'S ATMOSPHERE

T. del Río-Gaztelurrutia[1], A. Sánchez-Lavega[1], A. Antuñano[1], J. Legarreta[2], E. García-Melendo[3], K. M. Sayanagi[4], R. Hueso[1], M.H. Wong[5], S. Pérez-Hoyos[1], J.F. Rojas[1], A. A. Simon[6], I. de Pater[5], T. Barry[7]

[1]Departamento Física Aplicada I, Escuela de Ingeniería de Bilbao, UPV/EHU, Pl. Ing.Torres Quevedo 1, 48013 Bilbao, Spain.
[2] Sistemen Ingeniaritza eta Automatika Saila, Bilboko Ingeniaritza Eskola, UPV/EHU, Rafael Moreno "Pitxitxi",3, 48013 Bilbao, Spain.
[3]Escola Superior d'Enginyeries Industrial, Aeroespacial i Audiovisual de Terrassa, Universitat Politècnica de Catalunya (Barcelona Tech), Colom 11, 08222 Terrassa, Spain.
[4]Department of Atmospheric and Planetary Sciences, Hampton University, Hampton, VA 23668, USA
[5]University of California, Department of Astronomy, 501 Campbell Hall, Berkeley, California 94720, USA
[6]NASA Goddard Space Flight Center/690, 8800 Greenbelt Road, Greenbelt, Maryland 20771, USA
[7]Broken Hill Observatory, 406 Bromide Street, Broken Hill, New South Wales 2880, Australia

Keywords
Saturn; Atmospheres, dynamics; Saturn, atmosphere; Hubble Space Telescope observations

Abstract
The zonal wind profile of Saturn has a unique structure at 60ºN with a double-peaked jet that reaches maximum zonal velocities close to 100 ms^{-1}. In this region, a singular group of vortices consisting of a cyclone surrounded by two anticyclones was active since 2012 until the time of this report. Our observation demonstrates that vortices in Saturn can be long-lived. The three-vortex system drifts at u=69.0±1.6 ms^{-1}, similar to the speed of the local wind. Local motions reveal that the relative vorticity of the vortices comprising the system is ~2-3 times the ambient zonal vorticity. In May 2015, a disturbance developed at the location of the triple vortex system, and expanded eastwards covering in two months a third of the latitudinal circle, but leaving the vortices essentially unchanged. At the time of the onset of the disturbance, a fourth vortex was present at 55ºN, south of the three vortices and the evolution of the disturbance proved to be linked to the motion of this vortex. Measurements of local motions of the disturbed region show that cloud features moved essentially at the local wind speeds, suggesting that the disturbance consisted of passively advecting clouds generated by the interaction of the triple vortex system with the fourth vortex to the south. Nonlinear simulations are able to reproduce the stability and longevity of the triple vortex system under low vertical wind shear and high static stability in the upper troposphere of Saturn.

1. Introduction

Vortices in Saturn are difficult to see from ground-based telescopic imaging because of their relatively small size and low albedo contrast. Prior to Cassini spacecraft's arrival to the planet in 2004, most Saturnian vortices were detected either during the Voyager flybys in 1980-81 (Smith et al., 1980, 1981; Ingersoll et al., 1984; Sánchez-Lavega et al., 1993, Sanchez-Lavega et al., 1997; García-Melendo and Sánchez-Lavega, 2007), or in observations taken by the Hubble Space Telescope (HST) (Sánchez-Lavega et al., 2003, 2004). Since 2004, Cassini has provided a more continuous coverage of the atmospheric features of the planet. Several studies have analyzed the size, morphology, lifetime and latitudinal distribution of different vortices observed by the Imaging Science Subsystem (ISS) (Vasavada et al., 2006, Del Genio et al., 2009, del Río-Gaztelurrutia et al., 2010, Sayanagi et al. 2013, 2014, Trammell et al., 2014) and by the Visual and Infrared Mapping Spectrometer (VIMS) instrument (Baines et al., 2009; Dyudina et al., 2007). These analyses provide important clues on the large-scale dynamics of Saturn's atmosphere (Trammell et al., 2014, Trammell et al., 2016). In particular, numerical modeling of these systems shows the atmospheric conditions at deep levels of the weather layer under which the Saturn vortices are stable (García-Melendo et al., 2007, del Río-Gaztelurrutia et al., 2010). Thus, the existence and evolution of long-lived vortices are key to understanding the atmospheric conditions beneath the observable upper clouds.

The zonal wind profile of Saturn, like that of Jupiter, is approximately symmetric in latitude, with a strong prograde (eastward) equatorial jet and four other eastward jets in the North and South hemispheres. The jet around +60º planetocentric latitude has a distinct double-peak structure and reaches maximum zonal velocities close to 100 ms^{-1} (Figure 1). This feature of the jet is stable in time: It was present in 1981, when the Voyagers' flybys allowed measurements of zonal wind with sufficient latitudinal resolution (Sánchez-Lavega et al., 2000) and it was also observed by Cassini (Vasavada et al., 2006; García-Melendo et al., 2011). However, this double-peak structure is not present in any other wind jet either in Saturn or in Jupiter (García-Melendo et al., 2001; Porco et al., 2003).

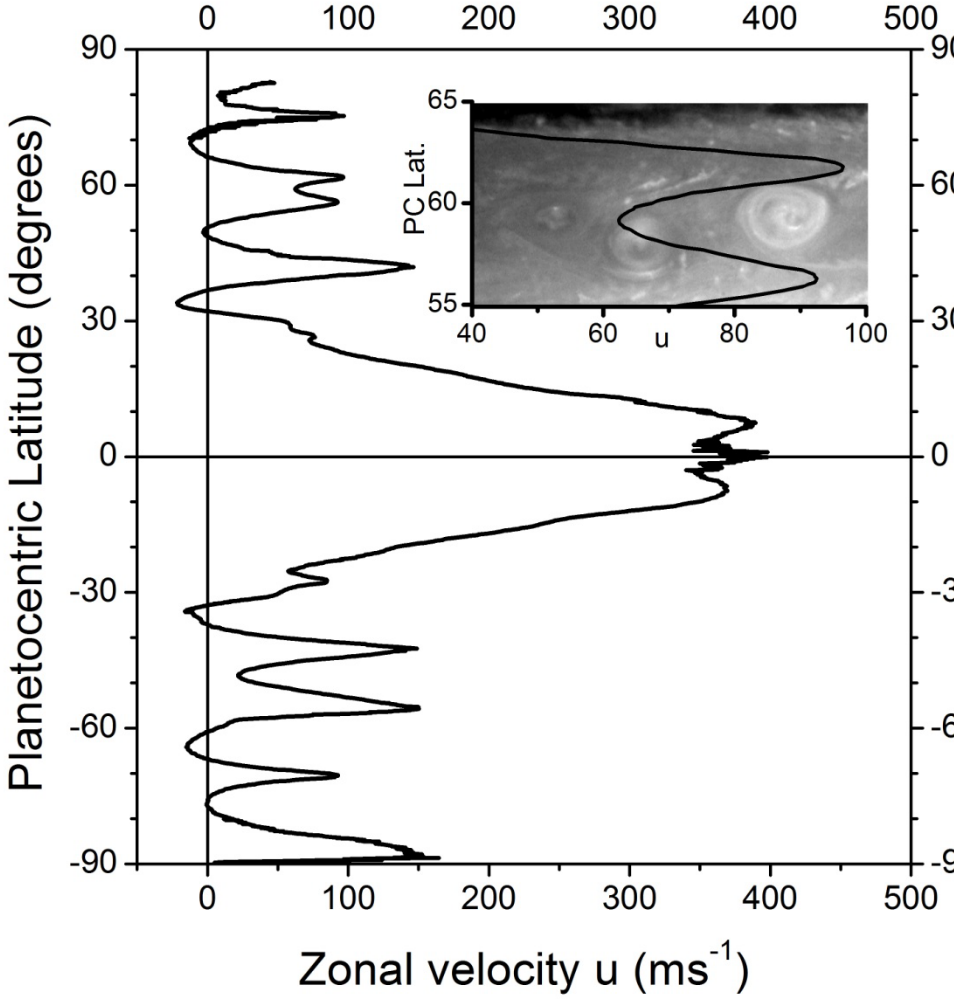

Figure 1. *Zonal wind velocity profile of Saturn. Inset shows the double peak jet between 55° and 65°N, together with a cylindrical projection of the triple vortex system.*

In Jupiter, cyclonic and anticyclonic vortices tend to form between jet peaks, in regions with low wind velocity and weak meridional vorticity gradient. These Jovian vortices drift at velocities not identical to the local winds (Simon and Beebe 1996, Li et al., 2004, Del Genio et al., 2009, Ingersoll et al. 2004). In Saturn, vortices have been observed drifting zonally at high velocities, and in regions with weak vorticity gradient, suggesting that cyclones and anticyclones tend to form close to the inflection point of the jet curvature $\left(d^2u / dy^2 = 0 \right)$ In the case of Saturn, the precise rotation rate of the planet has not been yet determined (Del Genio et al., 2009) but, as is standard, we adopt System III West longitudes (Archinal et al., 2011) to compute zonal winds. Although a change in the rotation period within the values proposed so far would change the values of zonal velocities, it would not change the meridionally alternating shape of the zonal wind profile (Sánchez-Lavega, 2005) and the values of vorticity. The twin peaks of the 60ºN jet mark two distinct dynamical regions, very close in latitude, with similar rather high eastward velocity but with opposite ambient vorticity. Thus, the jet structure in this region of Saturn facilitates the coupling of ovals of opposite vorticity North and South of the local minimum of velocity in the region of the double peak jet.

Trammel et al. (2016) analyzed Saturn's northern hemisphere from 2009 to 2015 and found that, with the exception of the large anticyclone that developed after the Great White Storm of 2010 (Sánchez-Lavega et al., 2012; Sayanagi et al., 2013), vortices had a lifetime of less than a year, and that the number of vortices varied in a significant way in the period of study. In their work, they did not concentrate in a particular region of the hemisphere, and their estimate of the lifetime of the vortices was based on temporal changes in vortex statistics rather than tracking individual vortices.

This work focuses on the region between 55 ºN and 65 ºN around the double peaked jet. We briefly describe the temporal evolution of the vortices in that region between 2007 and 2016 and then we focus our analysis on a long-lived system of one cyclone and two anticyclones that started interacting around 2012. This coupled system is still visible in images of Saturn at the end of 2016 and thus has survived for at least four years. In what follows, we shall refer to the triple vortex system as Anticyclone-Cyclone-Anticyclone abbreviated as ACA system (Figure 1, inset). In May 2015, a large disturbance developed at the location of ACA system, prominent enough to be observable in ground-based images captured with small telescopes. This disturbance expanded quickly in longitude following the zonal winds and covered approximately a third of the longitudinal circle. The disturbance faded by July 2015 but the ACA system survived and remained essentially unchanged, illustrating the remarkable stability of the system.

Other well-known cases of anticyclone-cyclone-anticyclone systems occurred on Jupiter during the mergers of White Ovals at 33ºS latitude that eventually became the present-day Oval BA (Sánchez-Lavega et al 2001, Hueso et al 2009). These ovals, nicknamed BC, DE and FA, formed around 1940 as long elongated white sectors in a Jovian band and then shrunk progressively until they reached about 10,000 km in the east-west direction (see e.g. Rogers, 1995). During their lifetime, these ovals wandered in longitude, approaching and separating as if they repelled each other. In 1998, BC and DE approached very closely; initially, a cyclonic cell between them impeded their approach, forming a compact anticyclone-cyclone-anticyclone system. However, subsequent interaction of the northern edge of the three vortex system with the southern edge of Jupiter's Great Red Spot (GRS) displaced the cyclone meridionally and led to the merger of BC and DE, forming BE (Sánchez-Lavega et al, 1999). One year later, a merger between BE and FA followed a similar sequence of events and formed the anticyclone BA (Sánchez-Lavega et al, 2001), still present in the atmosphere of Jupiter (Simon et al., 2015). The longevity of the vortices and their sudden merger was explained by Youssef and Marcus (2003), while the cause of an intriguing and lasting change in color from white to red has been addressed by, e.g., de Pater et al., 2010; Wong et al., 2011; Marcus et al., 2013.

The objective of the research presented in this paper is to conduct a detailed study of Saturn's ACA system and the disturbance that developed at the location of the system in May 2015, in an attempt to establish its origin. In section 2, we describe our data and methods of analysis. In section 3, we establish the lifetime and long time evolution of the ACA system and in section 4, we present its morphology and local motions. Section 5 is dedicated to an analysis of the perturbation that developed in May 2015. In section 6, we include some numerical analyses of the stability of vortices in the double peaked jet. In section 7, we summarize our conclusions.

2. Data and Methods

The images we analyze in this work can be classified in three sets. A first set comprises images taken by the ISS instrument onboard Cassini (Porco et al., 2004) using both the Wide Angle Camera (WAC) and the Narrow Angle Camera (NAC). Those images have a wide range of spatial resolutions and are mostly captured at filters covering methane absorption bands MT2, MT3 and their corresponding continuum filters CB2 and CB3, which allow easier identification of the features under analysis. They cover the period 2007-2016. A second set includes three groups of images taken with a variety of filters in three different orbits by the Wide Field Camera 3 (WFC3) onboard HST, on June 29-30 and July 1, 2015 (Sánchez-Lavega et al., 2016). A final set of images consists of images retrieved from the International Outer Planets Watch (IOPW) network hosted at the Planetary Virtual Observatory and Laboratory (PVOL) database[1] (Hueso et al., 2010a, 2017), which provides access to very good quality planetary images obtained by amateur astronomers. In Table 1, we present a summary of the images used in this study.

Table 1: Summary of the images used in this study.

Local motions and morphology description of the ACA system				
Instrument	*Filters*	*Date*	*Resolution* (km/pixel)	*N*
Cassini ISS (WAC and NAC)	CB2 / MT2	27 Feb 2013	36/72	4
	MT3	9 Feb 2015	120	1
	MT3	25 May 2015	140	1
	MT3	7 Sep 2015	227	1
HST WFC3	FQ937N/ FQ889N F336W	29 Jun -1 Jul 2015	300	5

Morphology of the cyclone				
Instrument	*Filter*	*Date*	*Resolution* (km/pixel)	*Phase Angle*
Cassini ISS (WAC and NAC)	CB2	13 Jan 2008	68.3	58.5
	CB2	21 Jan 2009	51.6	55.4
	CB2	25 Jul 2010	60.7	29.6
	CB2	27 Nov 2012	39.2	12.5
	CB2	17 Aug 2013	63.1	26.2
	CB2	3 Apr 2014	12.4	38.0

Long term tracking			
Source	*Dates*	*Resolution* (km/pixel)	*N*
Cassini ISS WAC	8 Jul 2007 – 8 Sep 2015	36 - 450	78
HST WFC3	29 Jun 2015- 1 Jul 2015	300	9
IOPW-PVOL	30 Jan 2015- 19 Sep 2015	1000	69

Images obtained by Cassini ISS are navigated using the software PLIA (Hueso et al., 2010b). This software uses SPICE kernels to assign latitude and longitude to each image pixel, and allows fine adjustment of the navigation when the limb is visible in the image. The HST/WFC3 images are navigated with Simnav, a custom-made software written in

[1] The PVOL database is available at http://pvol2.ehu.eus

IDL, which assigns latitude, longitude, emission, and incident angle values to each pixel by aligning a synthetic planetary disk to the science data (Lii et al. 2010). This method treats images as orthographic projections, and achieves subpixel alignment accuracy. Finally, images from the PVOL database were navigated via limb-fitting using the software LAIA (http://www.ajax.ehu.es/). Throughout this report, latitudes are planetocentric and longitudes are in Saturn System III (Archinal et al., 2010).

Low-resolution PVOL images and Cassini ISS WAC images are used in combination for the long-term analysis of the ACA system. Errors in latitude in the analysis of the long-term motion are represented by the standard deviation of the values of the whole data set. The average zonal velocity is deduced from the linear fit to the longitudinal drift using the expression:

$$u = R(\varphi_{PC})\cos\varphi_{PC}\frac{d\lambda}{dt} \tag{1}$$

where u is the zonal velocity, φ_{PC} is the planetocentric latitude, $R(\varphi_{PC})$ the radius of Saturn at latitude φ_{PC} and $d\lambda/dt$ the drift in longitude measured in radians per second. The long temporal intervals involved imply that the error in the determination of the mean longitudinal drift is very small, and the main error in zonal velocities arises from the error in the determination of the latitude, since at the high latitudes involved in this study, the length of the longitudinal circle varies strongly with latitude. We have estimated the error in velocity using the expression:

$$\Delta u \approx u \tan\varphi_{PC}\Delta\varphi_{PC}\,, \tag{2}$$

leading to errors of the order of 1.5 ms^{-1} for a typical error of 0.7º in latitude and a velocity of 70 ms^{-1}.

Local wind speeds are measured in the high-resolution Cassini ISS WAC images and HST WFC3 images assuming that cloud features advect with the local wind as passive tracers. We have used a combination of two different methods to measure wind speeds: manual cloud tracking of individual features and a supervised brightness correlation method (Hueso et al. 2010b). To analyze the cloud motion inside of the ACA system in high resolution, we analyze pairs of Cassini ISS images separated in time by approximately two hours. The images are first transformed in cylindrical map projections (Snyder, 1987), and analyzed using the supervised brightness correlation method to determine the zonal and meridional displacement of trackable features. In this case, due to the short time interval between the images, the main source of error in the determination of velocities is navigation uncertainty. We determine the uncertainties of those measurements using the pixel scale p and the time interval between images Δt as $\Delta u \approx p/\Delta t$ for one-pixel uncertainty on the location of the navigation grid, which makes the total uncertainty approximately 5 ms^{-1} in our analysis of CB2 images of February 2013.

In the analysis of the planetary disturbance, we analyze HST/WFC images that cover a large portion of the planet with images separated by two Saturn rotations. The images are mapped in polar projections to allow easier identification of the features. In this case, zonal winds have been measured using visual cloud tracking of the most prominent features. Whenever possible, linear fits to the cloud motions are performed to determine their long-term mean motion. Error in those measurements is due mainly to the inferior resolution and uncertainties in the feature positions due to the evolution of the identified features, and it has been estimated as $\Delta u \approx d / \Delta t$, where d is the estimated uncertainty in a feature position, leading to a combined uncertainty of approximately 4 ms^{-1}.

3. History of the ACA vortex system

In order to study the long-term evolution of the ACA system, we surveyed Cassini images of Saturn's Northern sub-polar latitudes surrounding the double-peaked jet, from 50º to 65º planetocentric latitude (see Figure 1). The first Cassini views of this region were obtained in mid-2007, showing a number of moderately sized but well-formed vortices. Vortices of similar appearance can be identified up to the end of 2015 whenever the region was visible by Cassini at enough spatial resolution but there are significant large gaps in the temporal coverage of these latitudes.

At the latitudes corresponding to the cyclonic region of the double peak jet, ~58.5ºN (the region south of the westward local minimum in the zonal wind) images captured in July 2007 show the presence of an oval-shaped vortex. All later maps of this latitudinal band at high enough spatial resolution reveal the presence of just one similar vortex at that latitude. Figure 2 shows those cyclones at six different epochs, showing that while there are some changes in the cloud morphology, there are no great changes in size or general aspect, reminiscent of the long-lived cyclone tracked during four years (2004-2008) in Saturn's South Hemisphere (del Río-Gaztelurrutia et al., 2010). In the present case, an attempt to check if all images correspond to one cyclone that has survived during the 2007-2015 time period is hindered both by the sparse sampling of the data, particularly in the years 2009-2012, with very long temporal gaps with no images of the region, and the relatively high zonal velocities, ranging from 60 to 95 ms^{-1} (Figure 1). In the high latitudes under study, such velocities imply that a vortex can circumnavigate a whole latitudinal circle in a month. More specifically, if we assume that the vortex moves with the wind profile, a change of latitude of 0.1º would imply a change of velocity of 1.5ms^{-1}. If such a change of latitude occurs in a period when there are no images, the longitude of the vortex could drift as much as 8º per month from the expected longitude, making the identification uncertain for a typical time interval of the order of half a year.

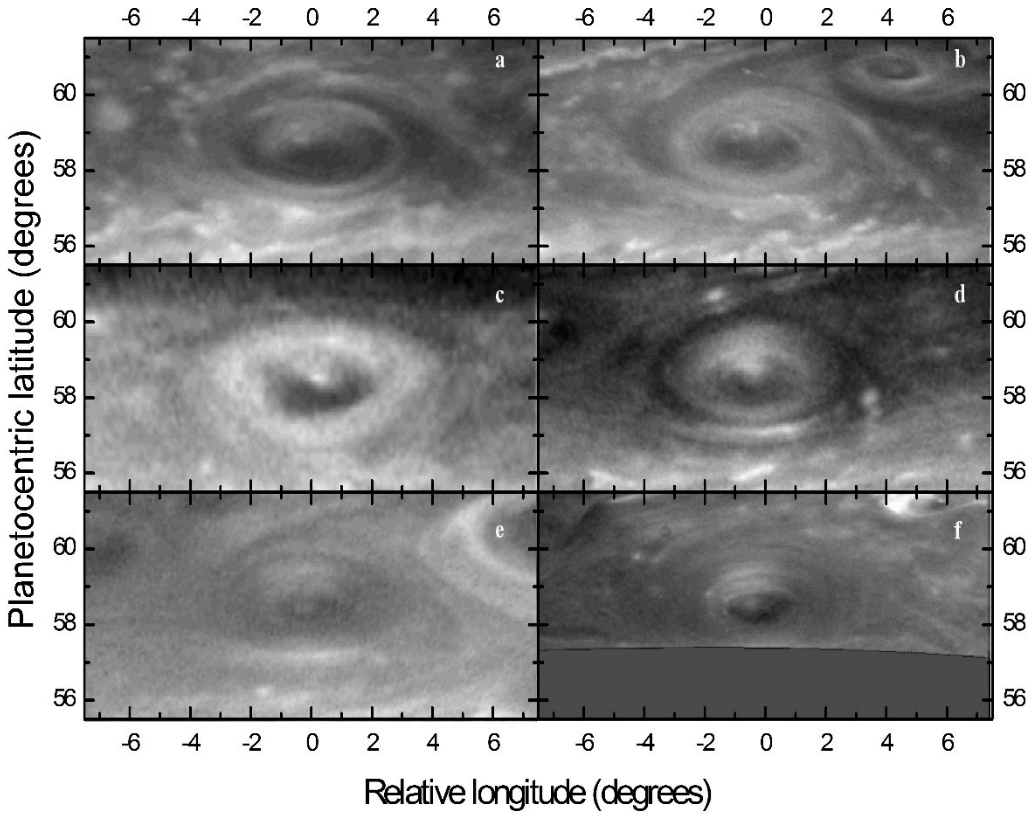

Figure 2: *Cylindrically projected maps of the cyclonic vortex at 58.5ºN. Images were captured by Cassini ISS WAC with the CB2 filter, with the exception of panel f, which corresponds to a NAC image also acquired with the CB2 filter. Dates for each panel are: (a) 13/01/2008 (b) 21/1/2009 (c) 25/7/2010 (d) 27/11/2012 (e) 17/8/2013 (f) 03/04/2014. Phase angle and pixel scale of original images are indicated in Table 1*

At higher latitudes, ~60ºN, in the anticyclonic region of the double peaked jet (i.e. the region to the north of the westward minimum of the zonal wind), a varying number (from 1 to 3) of similarly sized vortices are detected during the 2007-2015 period. Again, the long temporal gaps between the images make it difficult to identify uniquely any of these drifting vortices, all of very similar appearance.

Nevertheless, at some point in 2012 the cyclone came in close contact with two anticyclones located at latitude 60ºN, forming a stable triple vortex structure. This triple vortex formation is very distinct, and therefore much easier to track, particularly in the deep methane absorbing filter MT3, in which even a moderate resolution image shows the cyclone as a compact circular dark spot and the adjacent anticyclones as two bright spots. Moreover, perhaps due to the larger overall size of the ACA system combined with the higher resolution of amateur images, it was possible to detect the feature, appearing as a spot at the position of the ACA system, in amateur images from the beginning of

2015. We can thus continuously track the ACA system from the beginning of 2012 until at least 31st of July 2016, where its tripolar structure is apparent in very high quality amateur images available at the PVOL database.

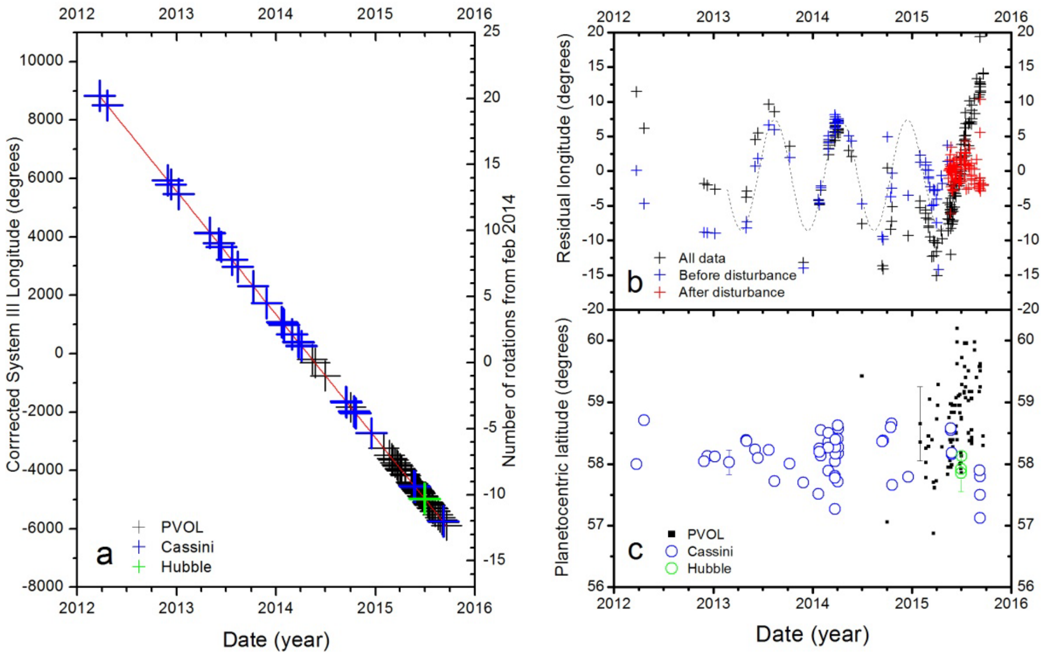

***Figure 3. Panel a**: Longitudinal drift in System III of the centroid of the cyclone in the ACA system. An appropriate number of full rotations has been added to the longitude, as indicated in the axis at the right of the panel. The red line is the linear fit of the data. **Panel b:** Residuals of the linear fit to the longitude drift. In black, the residuals of the fit of all data, in blue the residuals of the fit previous to the onset of the disturbance and in red the residuals of the fit after the perturbation. The dotted sinusoidal line represents the approximate oscillations before the onset of the disturbance. **Panel c:** Latitude of the centroid of the cyclone. Typical errors in the measurements are indicated in selected points.*

Figure 3a presents the longitude of the centroid of the cyclone at the center of the ACA system from the end of 2012 to mid-2016, tracked using Cassini ISS images taken with the MT3 and MT2 filters from 2012 to the end of 2015, amateur images from the beginning of 2015 to the end of 2015, and Hubble images from June-July 2015. Due to the fast drift rate of this feature, we present our measurements in a modified longitude system that takes into account the continuous circumnavigating motion of the feature. There are long temporal gaps in the data, but the presence of the neighboring vortices makes the identification of the cyclone certain, and the number of complete circumnavigations accounted in the modified System III longitudes in order to calculate the average drift can be unambiguously deduced because of the long temporal tracking record.

When all data are taken into account, the average planetocentric latitude of the cyclone is 58.5º±0.8ºN and it drifts in longitude at -11.55º/day, corresponding to an average zonal velocity of u=69.0±1.6 ms^{-1} at this latitude. Figure 3b shows the residuals from this linear fit as black points. The figure shows a clear change in the residual motion at the onset of the disturbance in May 2015. If we take into account the data up to mid May 2015 into account, the numbers are very similar (average latitude is 58.2º±0.5ºN, and the average drift is -11.56º/day, and corresponding a zonal velocity of u=68.8±1.0 ms-1). The residuals of this fit are plotted in blue in Figure 3b. After the onset of the disturbance, the average latitude is 58.9º±0.8ºN and the longitudinal drift 11.36º/day, leading to a slight change in velocity, of u=66.1±1.5 ms^{-1}. We also note that, before the onset of the disturbance, the residuals of the fit show a roughly periodic behavior of amplitude ~10º and a period of ~8 months superposed to the average zonal motion. This oscillation could be correlated with an oscillation in latitude, but the noise in the latitudinal data does not allow us to conclude whether this is indeed the case. In Figure 3c, we show the measured latitudes as a function of time, showing data points from small-size telescopes, Hubble and Cassini in different symbols. It is apparent that ground-based PVOL data after the onset of the disturbance reflect higher latitudes than data from Cassini or Hubble. This is probably an artefact due to the lower resolution of the images, which biases the latitudinal measurement toward the center of the ACA system rather than the center of the cyclone; the cyclone's latitude is always lower than those of the anticyclones (and the center of the ACA system) whenever the whole system is visible in an image.

We have also tracked the longitudinal drift of the centroid of the two anticyclones using only Cassini and Hubble data. Both vortices drift at essentially the same zonal velocity. The leading anticyclone, to the east of the cyclone in the ACA system, is located at an average latitude of 59.6º±1.0ºN and drifts at -11.54º/day, corresponding to an average zonal velocity of u=65.6±1.9 ms^{-1}, and the trailing anticyclone, to the west of the cyclone, is at the same average latitude 59.6º±0.9ºN and drifts at -11.53º/day, corresponding to an average zonal velocity of u=65.7±1.9 ms^{-1}.

Figure 4 compares the main drift rate of the vortices at different epochs with the zonal winds, showing that they are very close to the zonal wind speeds but slightly offset, and shows the small changes in the drift rate of the cyclone before and after the onset of the disturbance.

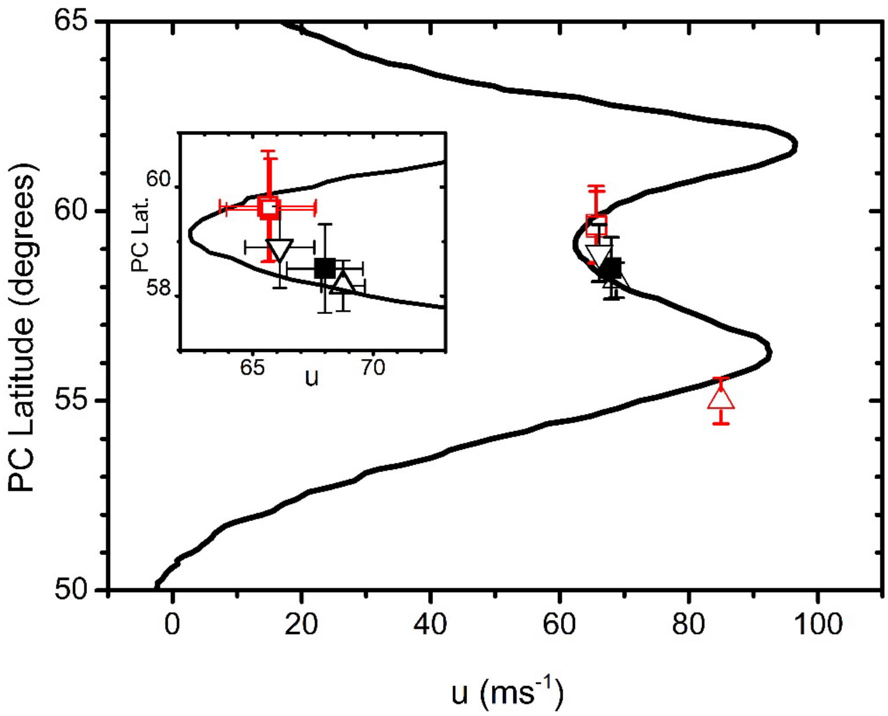

Figure 4. *Latitude and velocity of each element of the ACA system compared to Saturn's zonal wind profile. The black filled square indicates the mean latitude and velocity of the*

cyclone (2012-2016). Upward-pointing triangle represents the average latitude and velocity before the onset of the disturbance (2012-May2015) and the downward-pointing triangle is the results after the onset of the disturbance (May-Dec 2015). The two closely placed red squares represent the average latitude and zonal drift of the two anticyclones of the ACA system and the red triangle indicates an anticyclone at 55ºN that will be discussed below. Zonal wind profile is the one given in García-Melendo et al (2011).

Although the ACA system is stable, the relative separation between the vortices changes in time. Over the studied period, the longitudinal separation between the centers of the two anticyclones was on average ~25 degrees, oscillating between a minimum of 16º and a maximum of 35º. On the other hand, the location of the cyclone oscillated, alternately approaching the two anticyclones. Figure 5 shows the variation in time of the relative locations of the three vortices.

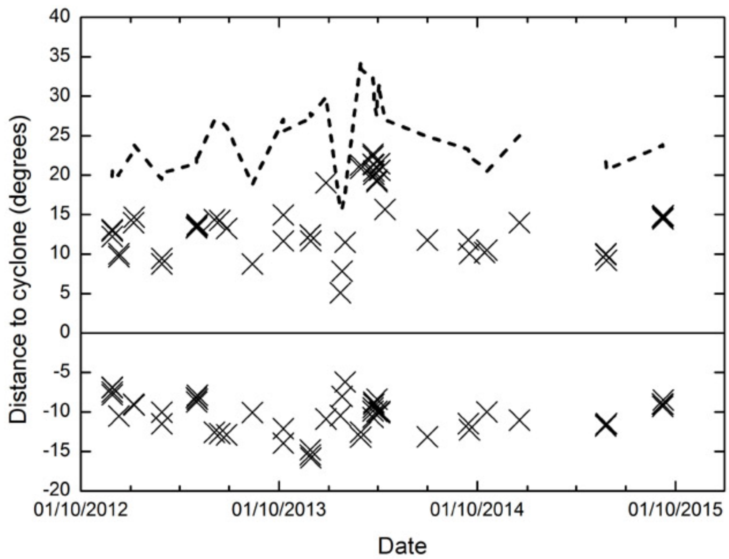

Figure 5. *Relative distances in the ACA system. Dashed line indicates the separation between the two anticyclones between 2012 and 2015 based on Cassini ISS position measurements. The crosses represent the individual distance of the anticyclones to the cyclone placed at the continuous horizontal line at 0 degrees. The western (i.e. trailing) anticyclone is represented by the negative positions.*

4. Morphology and local motions of the ACA system

4.1. The ACA system

Figure 6 presents the appearance of the ACA system in CB2 and MT3 filters. Asay-Davis et al. (2009) showed that the sizes measured visually from the cloud appearance of Jovian vortices could be different than the dynamical sizes (as defined by the ring of maximum speed), and for example, the size of the Great Red Spot on Jupiter shrinks at different rates, depending on whether cloud appearance or dynamics is used to define the size (Simon et al. 2014). In this study, we define vortex size by cloud appearance, and uncertainties in size parameters correspond to the intrinsic spatial resolution of the Cassini and HST data. The size of the vortices that compose the system has not changed appreciably in the period of the study from the beginning of 2012 until the end of 2015.

In CB2 images, the cyclonic vortex extends 3.1±0.4º in latitude and 6.8±0.5º in longitude, corresponding to an essentially circular vortex of dimensions 3,100±400 km (North-South) × 3,400 ± 300 km (East-West), while in MT3 only the inner region is visible, extending 1.8±0.3º in latitude and 4.2±0.8º in longitude, corresponding to 1,800±300 km (North-South) × 2100±400 km (East-West). In all images, the anticyclonic vortex to the east is larger and has a higher contrast than the anticyclone to the west. The eastern anticyclone extends 2.6±0.6º in latitude, and 6.6±1.2 º in longitude, corresponding to 2,600±600 km (North-South) × 3,300±600 km (East-West). The western anticyclonic vortex extends 1.8±0.5º in latitude and 4.8±0.8 in longitude, corresponding to 1,800±500 km (North-South) × 2,400 ± 400 km (East-West).

As we have mentioned above, the system appears most conspicuous in methane absorption filters MT3 and MT2. In MT3 images, the cyclonic vortex in the middle of the system appears as a very compact spot dark relative to surroundings, indicating the presence of a thicker layer of atmosphere above the clouds. This suggests that the clouds that are visible in the continuum, possibly related to upwelling motions within the cyclone, are located deeper in the atmosphere than clouds and hazes in neighboring regions. This is consistent with its latitudinal location in the cyclonic region of the double peaked jet. The leading and trailing anticyclonic vortices appear bright, suggesting that they are structures high in the atmosphere, as expected of anticyclones, again consistent with their location in the anticyclonic latitudes of the double peaked jet. We have not found high-resolution images in those filters, but in moderate resolution images (Figure 6) the interiors of (1) the cyclone and (2) both anticyclones are essentially featureless dark and bright regions respectively. This combination of a very dark compact spot surrounded by two bright regions is easily recognizable, and has aided in the identification of the system even in low resolution images allowing the long-time track of the system.

In the continuum filters CB2 and CB3, the contrast between the ACA system and the surrounding regions is much lower, making it much harder to detect, particularly in images captured in equatorial orbits, where the sub-polar region is viewed tangentially. More inclined orbits allow a better view of the high-latitude region, and in Figure 6, we show the appearance of the ACA system in a medium resolution image captured on February 27, 2013. It shows the central cyclone as a low-contrast, slightly dark structure suggestive of a vertical depression in the clouds, with numerous small white features in the center, and bright clouds at the outer edge. Its visual appearance is very reminiscent of that of a long-lived cyclone in the Southern hemisphere (del Río-Gaztelurrutia et al., 2010). The accompanying anticyclones appear darker with a white collar surrounding them and bright features in the center. The only significant changes in the appearance of the ACA system in different periods are the number of bright features in the darker interior of the two anticyclones.

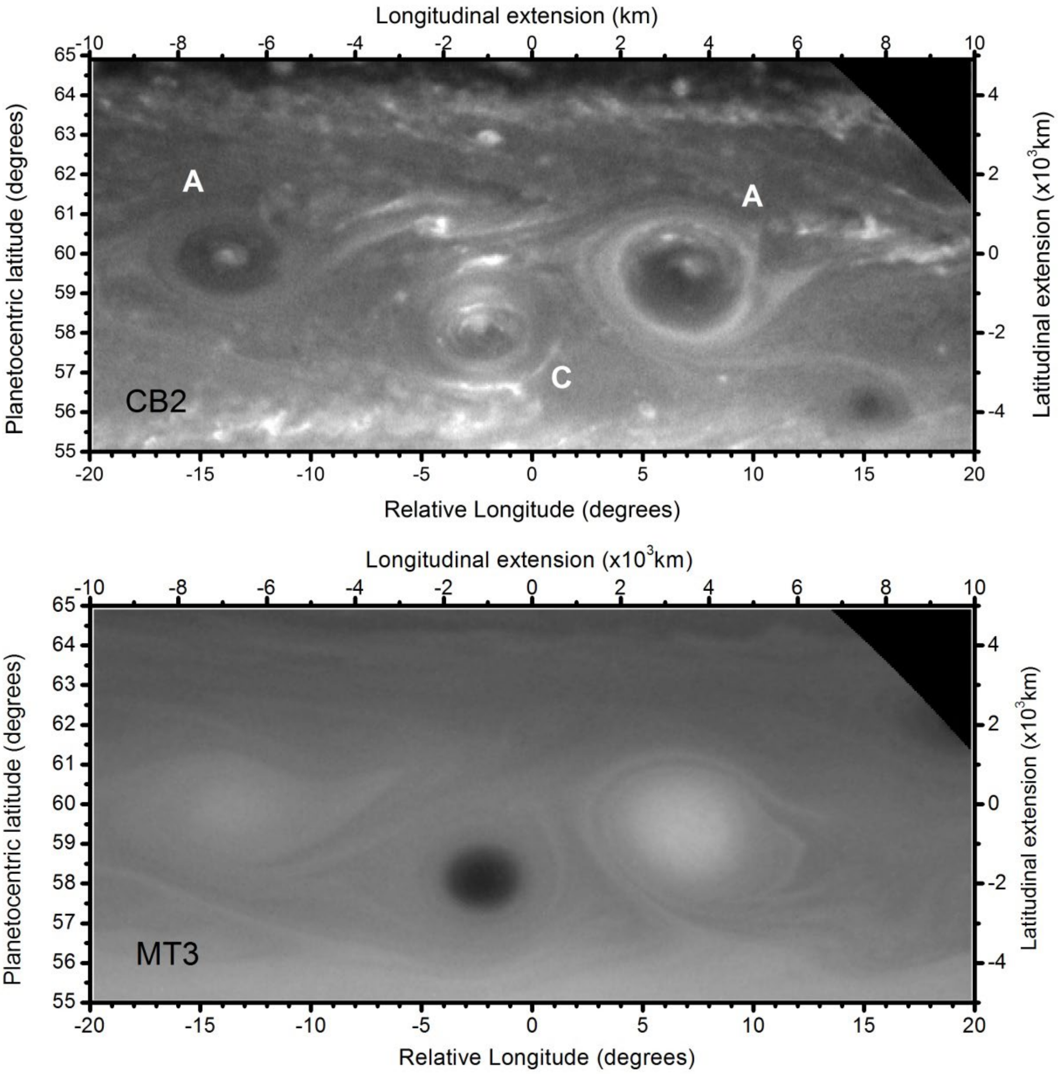

Figure 6. *Map projections of the ACA system in CB2 and MT3 filters. Original images were taken at a short time interval on 27 February 2013, and are labeled in the PDS database as W1740625129 (CB2) and W17406251112 (MT3).*

4.2 Local motions and vorticity.

Local motions inside the ACA system have been measured using a pair of medium resolution images captured with the ISS/WAC using the CB2 filter on February 27 2013 with a temporal interval of 2 hour 13 second. The original images (W1740617916 and W1740625129) have sub-spacecraft pixel scales of 36.7 km/pixel and 31.17 km/pixel, respectively. The images were projected to a resolution of 0.05º/pixel, which corresponds to a meridional spatial resolution of 25.1 km/pixel and a zonal spatial resolution of 48.7 km/pixel at 59ºN. The navigation s corrected via small deviations of the grid to ensure that average zonal winds outside the ACA system agree with the values past measurements by García-Melendo et al. (2011). This technique is further described in García-Melendo et al. (2011). There was a remaining uncertainty in image navigation of ±1 pixel, leading to an error in the velocity determination of ~ 10 ms^{-1}.

We used the software PICV2 (Particle Image Correlation Velocimetry software written in IDL) described in Hueso et al. (2010b), to retrieve local motions. Over 3,400 vectors were derived. In order to visualize the mean flow at the ACA system and calculate ambient vorticity maps, the measured velocity data were interpolated to a regular grid with a resolution of 0.5º. The results of this interpolation is shown in the upper panel of Figure 7, with the projection of the ACA system in the background.

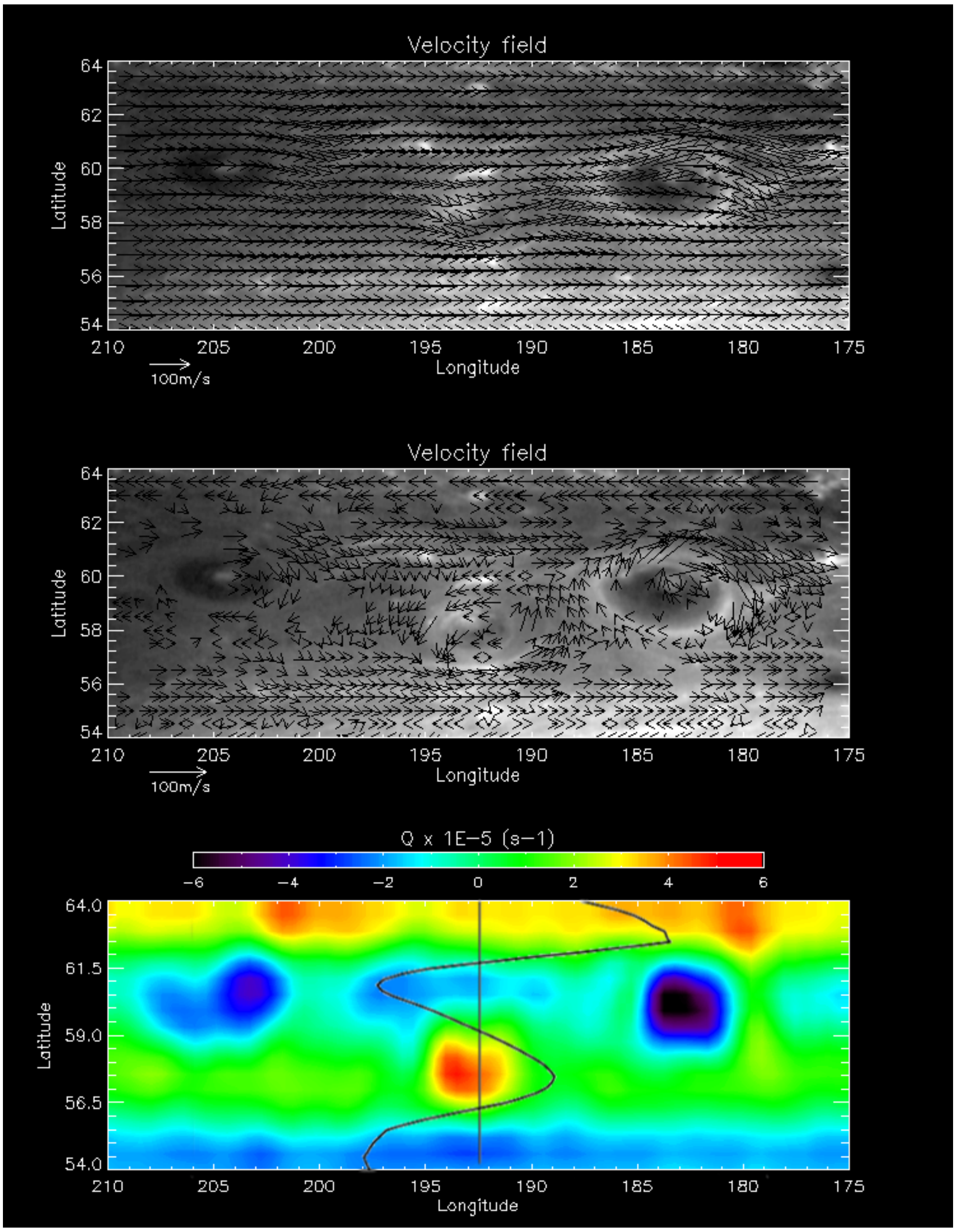

***Figure 7. Upper panel** shows the interpolated local wind field at the ACA system on 27 February 2013. Departures from zonal motion are apparent at the location of the cyclone and the larger anticyclone. Middle panel shows the local winds in the reference system of the cyclone, calculated subtracting the velocity of the centroid of the cyclone from all wind vectors, and averaged in bins of 0.5×0.5 degrees. In the **lower panel**, ambient vorticity is plotted using a color scale, with red indicating cyclonic and blue anticyclonic vorticities. The line indicates zonal ambient vorticity calculated using the zonal wind profile of García-Melendo et al. (2011), using the color bar as scale. The presence of the vortex at 58.5ºN is indicated as an intensification of cyclonic vorticity, up to ~ $4.5\times10^{-5}\,s^{-1}$. The anticyclones have maximum vorticity of ~ $-7\times10^{-5}\,s^{-1}$ (eastern anticyclone) and $-5\times10^{-5}\,s^{-1}$ (western anticyclone).*

Departures from zonal motion are evident in Figure 7. In order to estimate their magnitude, we have performed averages of meridional motion in longitudinal bins of 0.67º (Figure 8). In the cyclonic region from 56.4ºN to 59ºN, we find peak values of 16±9 ms^{-1}, separated by ~4º in longitude, while in the anticyclonic band from 59ºN to 61.8ºN, we find two oscillations, one with peak values of 36±10 ms^{-1} separated by ~5º in longitude corresponding to the eastern anticyclone and the other with peak values of 22±6 ms^{-1} separated by ~6º corresponding to the western anticyclone.

The enhancement of vorticity in the triple vortex system becomes apparent in the reference system of the centroid of the cyclone (Figure 7, middle panel), where the eddy circulation and the interaction between the vortices is more clearly seen. A crude estimate of the increase in local vorticity $\Delta\zeta$ from the local vorticity of the zonal winds can be obtained assuming that there is a circulation superposed to the zonal motion with constant tangential velocity Δv in a circle of radius *r*, using the formula:

$$\left|\Delta\zeta\right| \approx \frac{2\pi r \Delta v}{\pi r^2} = \frac{2\Delta v}{r}.$$

In order to estimate $\Delta\zeta$ for the three vortices, we use the maximum north-south component of the wind from Figure 8 as an estimate for the respective vortex's tangential wind velocity *v*, and the east-west distance between the meridional velocity peaks as an estimate for *r*. For the cyclone, we find $\Delta\zeta \approx (3\pm 2)\times 10^{-5}\,\mathrm{s}^{-1}$ and for the eastern and western anticyclones, we find $\Delta\zeta \approx -(5\pm 2)\times 10^{-5}\,\mathrm{s}^{-1}$ and $\Delta\zeta \approx -(3\pm 2)\times 10^{-5}\,\mathrm{s}^{-1}$, respectively. This simple estimation represents enhancements of vorticity over the local vorticity imposed by the meridional structure of the jet, and obviously ignores the interaction between vortices.

The interpolated velocity field allows us to calculate ambient vorticity maps using finite differences. The result is presented in the lower panel of Figure 7, where the line indicates zonal ambient vorticity in the region calculated from the zonal winds of García-Melendo et al. (2011), which ranges from $-2.5\times 10^{-5}\,\mathrm{s}^{-1}$ to $3.9\times 10^{-5}\,\mathrm{s}^{-1}$ in the region of the double-peaked jet. Even though spatially resolved maps of vorticity are noisy, the cyclonic and anticyclonic regions of the jets are retrieved in the vorticity map. At the region of the cyclone, vorticity rises from a zonal average of $1.5\times 10^{-5}\,\mathrm{s}^{-1}$ to $\sim 4.5\times 10^{-5}\,\mathrm{s}^{-1}$, approximately a sixth of the vertical component of planetary vorticity at the region. In the case of the anticyclones, enhancement from the zonal average of $-2.2\times 10^{-5}\,\mathrm{s}^{-1}$ is higher in the anticyclone at lower longitudes, which reaches a value of total local vorticity of $\sim -7\times 10^{-5}\,\mathrm{s}^{-1}$, while in the case of the anticyclone at higher longitudes, the total vorticity peaks at $\sim -5\times 10^{-5}\,\mathrm{s}^{-1}$. Those results are consistent with the crude estimations of the enhancement of local vorticity given above.

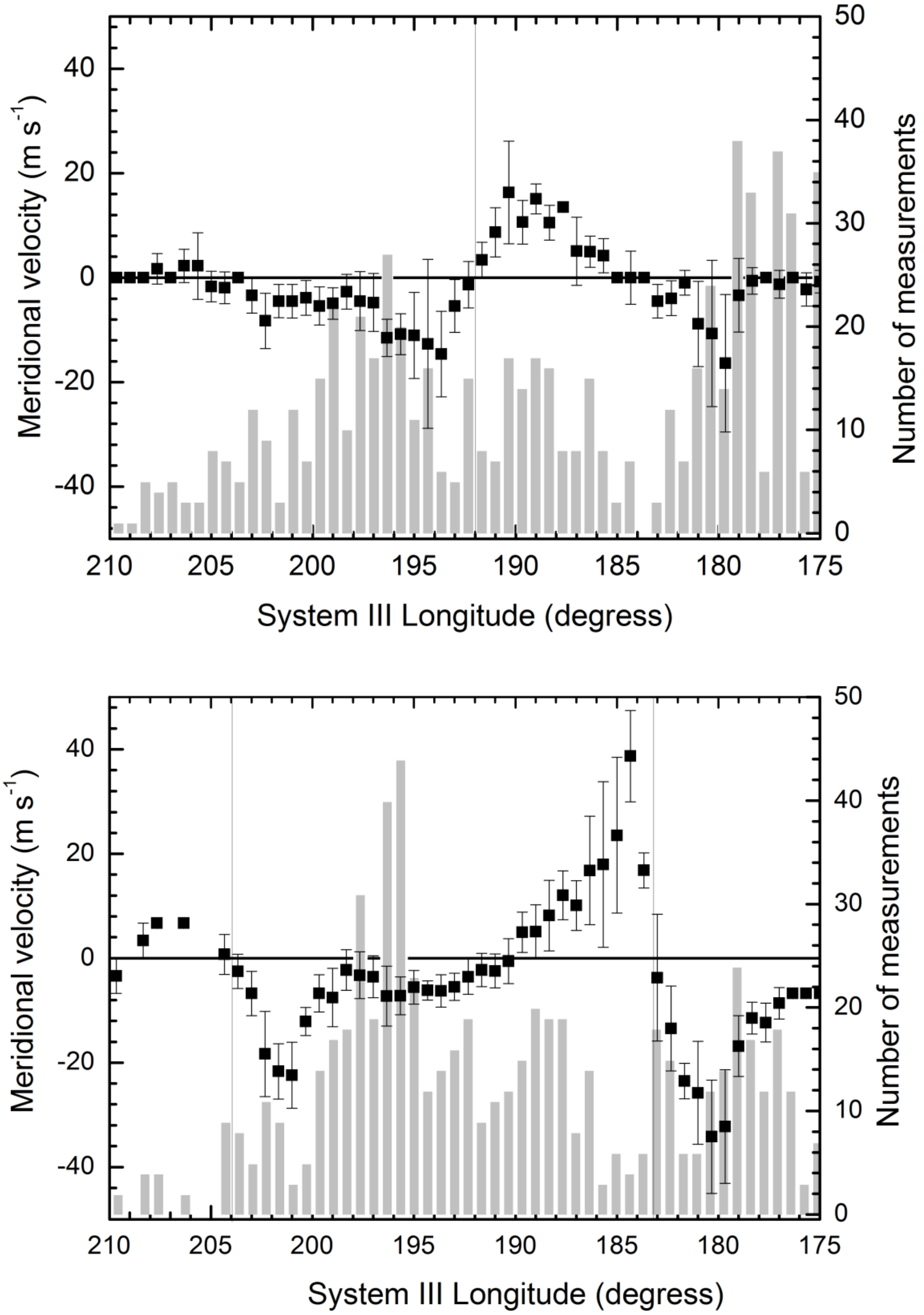

Figure 8. *Meridional velocity as a function of longitude obtained from longitudinal bins of 2/3 degrees (a compromise between resolution and the number of measurements per bin).* ***Upper panel:*** *results for the cyclonic latitudinal band from 56.4ºN to 59ºN.* ***Lower panel:*** *results for the anticyclonic band from 59ºN to 61.8ºN, displaying the two oscillations corresponding to the two anticyclonic vortices. In both plots, error bars represent the standard deviation and the bar chart indicates the number of measurements in each longitudinal bin.*

5. Planetary scale disturbance

5.1 Onset

The coupling of the three vortices, together with better viewing angles of Saturn northern latitudes, and recent improvements in planetary amateur astronomy techniques (Mousis et al., 2014) enabled a systematic observation of the ACA system since 2014, which generally appeared as a single dark spot in amateur images. On May 13, 2015, near Saturn opposition, the presence of a "rift" at the location of the spot captured the attention of the amateur community. Soon after, the region surrounding the spot appeared disturbed, and the perturbation extended longitudinally for approximately two months, at the end of which the perturbed region occupied about a third of the latitudinal circle (Figure 9).

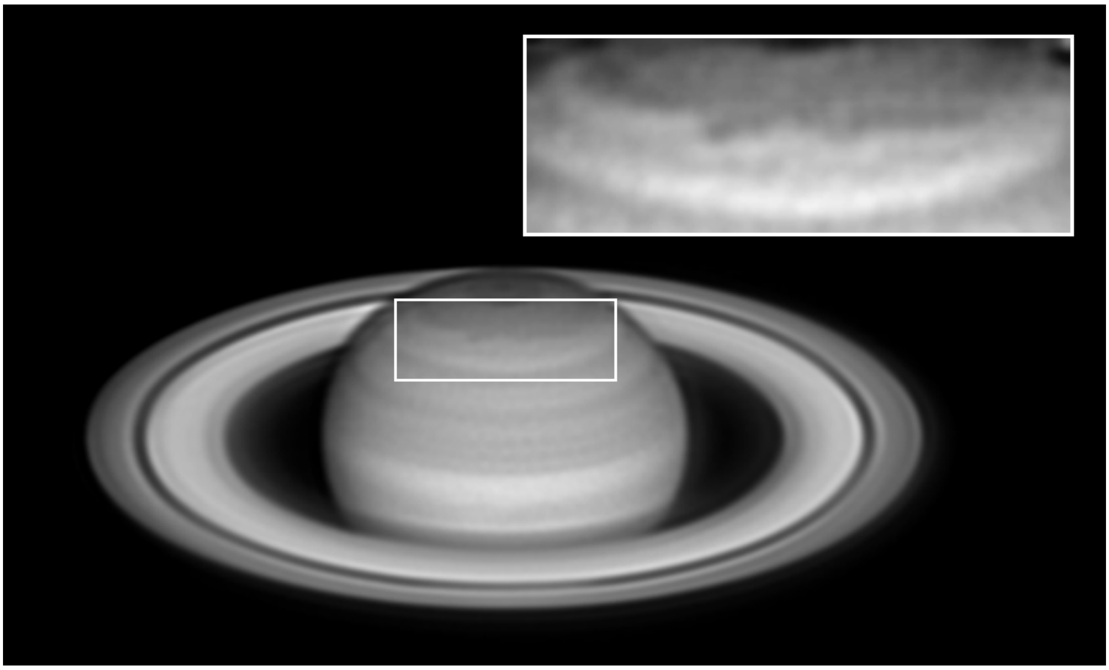

Figure 9. *Image of Saturn taken by T. Barry on 15 June 2015. The inset shows a zoom over the disturbed region and has been enhanced using high-pass filters. The image was captured with a 16" telescope using a 685nm IR pass filter. North is up and West to the left.*

There is just one set of high-resolution images of the region captured by Cassini ISS near the onset of the perturbation, on May 26, 2015. In these images (Figure 10a) a large vortex appears south of the ACA system, at ~55ºN, which could be the cause of the "rift" visible in amateur images. This vortex was also observed at high resolution at other dates before and after the onset of the disturbance (Figure 10b and 10c). Unfortunately, the geometry of Cassini ISS observations in the following months was not favorable to the observation of the system, with equatorial orbits and large phase angle illumination of the planet, and thus high resolution images of the region were not taken in that period.

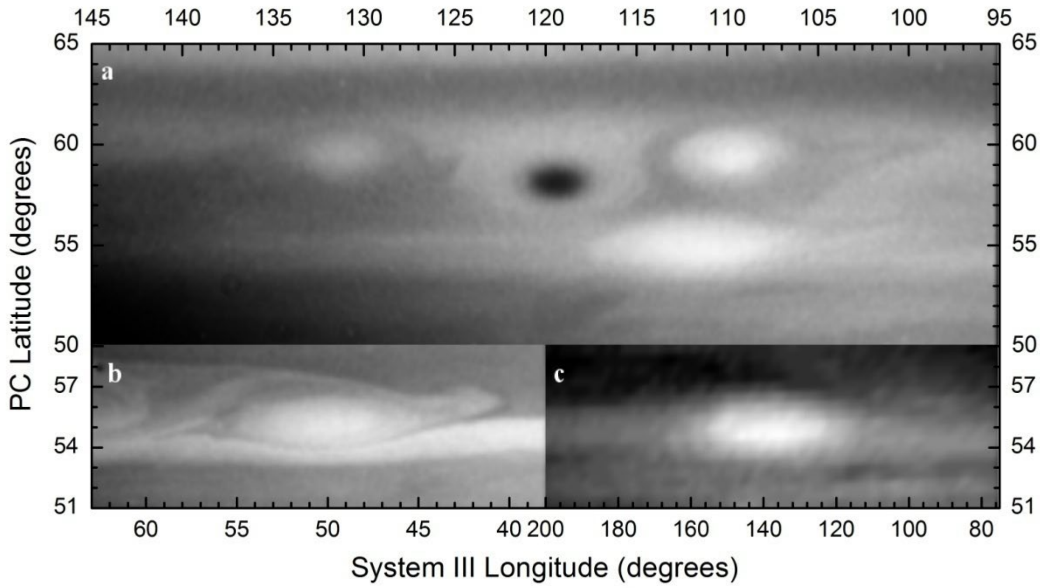

Figure 10. *Map projections of the ACA system and the vortex at 55ºN from images captured with the MT3 filter of Cassini ISS instrument.* ***Panel a:*** *The ACA system on 25 May 2015. The vortex at 55ºN is just south of the anticyclone at lower latitudes.* ***Panel b****: The anticyclone at 55ºN on 9 February 2015.* ***Panel c****: The anticyclone at 55ºN on 7 September 2015, 79º away from the longitudinal location of the ACA system at the time, 61º System III.*

5.2 Zonal evolution

The systematic survey of the region by amateur observers allowed the study of the global evolution of the disturbance. With this aim, the position of the spot visible in amateur images (corresponding essentially to the center of the ACA system) and the limits of the disturbed region were measured on selected images obtained from the PVOL database. The average drift of the spot during the observing period (May-Sep 2015) was -11.36º/day, corresponding to u=66 ms^{-1} at its average latitude of 58.8°N.

The longitudes of the edges of the perturbation in a reference system that moves with the spot are plotted in Figure 11a, where symbols indicate estimates of the edge of the perturbation and continuous lines represent linear fits to the best quality measurements. Figure 11a also shows the edges of the disturbed region in the high-resolution images of the region during the early period of the disturbance (HST/WFC3 observations discussed later). It is apparent from Figure 11a that the perturbation extended essentially eastwards with respect to the ACA system. The linear fit implies a mean relative drift of -1.65º/day, that is, the edge of the perturbation moved away from the ACA system at a relative velocity of ~12 ms^{-1}.

By mid-August, the latitudinal band had recovered an undisturbed appearance, while the spot marking the position of the ACA system remained visible.

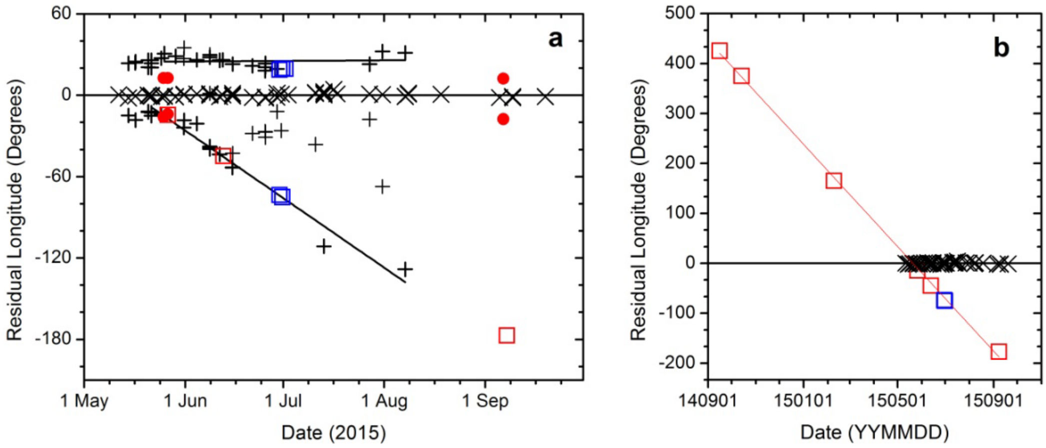

Figure 11. *Disturbance evolution with respect to the ACA system.* ***Panel a****: Longitudinal drift rate of the disturbance with respect to the ACA system at the time of the disturbance.* ***Panel b****: Longitudinal drift rate of the vortex at 55ºN in the reference system of the ACA system for an extended period of time. In both plots, crosses indicate the residuals of average drift of the centroid of the spot in amateur images during the disturbance. Blue squares denote the limits of the perturbed region in HST images to be discussed later. Red circles in panel* ***a*** *indicate the extension of the ACA system in Cassini ISS images captured with the MT3 filter. Red squares represent the position of the vortex at 55.5ºN.*

5.3. Drift of the vortex at 55ºN in the reference system of ACA

At the southern flank of the double-peaked jet, there is an anticyclonic band where Trammel et al. (2016) reported the presence of several vortices. Tracking the position of those vortices in time is not straightforward due to the fast zonal motions of this region, long time intervals with no data, and the very similar aspect of different vortices at the same latitudes.

At the time when amateurs reported “a rift” in the position of the ACA system, Cassini high-resolution images show the presence of one of those vortices south of the ACA system (Figure 10a). On September 6th-7th, 2015, when the disturbance had subdued, the region was again visible in Cassini ISS images. The viewing conditions of the images are not good, but the ACA system is clearly detected and the region east of it appears unperturbed. An inspection of the full latitudinal circle on that date reveals the presence of a large vortex at ~55ºN (Figure 10c) at the would-be longitude of the east edge of the perturbation. This suggests that the origin of the disturbance is the interaction of the ACA system with an anticyclonic vortex at lower latitudes drifting faster and therefore overtaking the ACA system, leaving the in-between region perturbed. In order to check this hypothesis, we have searched the Cassini database in 2014-2015 for detections of vortices at that latitudinal band, and plotted their longitudes in the reference system of the ACA system, where their relative velocity is lower, making identification easier. We have found that, indeed, the vortex can be traced back to August 2014, at an average latitude of 54.8 ±0.3ºN, approaching the ACA system at 1.70º/day (11.1±0.1ms^{-1}). The result of this tracking can be seen in Figure 11b. The zonal velocity of the vortex compared with the zonal winds is also indicated in Figure 4. This suggests that the disturbance observed in May 2015 was due to the interaction of the 55ºN vortex with the ACA system. The different drift velocities of the ACA system and the vortex at 55º imply that they cross each other every seven/eight months, but we have not found Cassini ISS images of the region at the time of other crossings and thus we cannot confirm or exclude the possibility that such an interaction occurs every crossing.

5.4. Disturbance 90 days after the onset: HST images

Due to the characteristics of Cassini orbits at the time, which did not allow us to observe the evolution of this disturbance, we requested HST observations of Saturn. HST observed Saturn on the 29th and 30th of June and the 1st of July 2015. HST WFC3 images of the region were captured approximately 40 days after the start of the disturbance. There are three sets of images, separated by two planetary rotations. In the first two sets, captured on the 29th and 30th of June, the ACA system is essentially on the sub-Earth meridian, and thus the images show the complete perturbed region. The third set, captured on July 1, the ACA system is closer to the limb and the eastern limit of the perturbed area is hidden from view. In Figure 12, we show three polar projections of the planet from images taken with the FQ937N, F889N and F336W filters on 29 June 2015. The first two filters are narrow band filters that have been chosen for their similarity to CB3 and MT3 filters in Cassini ISS, while the last one is a wide band filter providing images in the ultraviolet.

A comparison of the three images allows us to estimate the relative height of the different details and confirms that the ACA system consists of a cyclone surrounded by two anticyclones. Images in F889N in the strong methane absorption band and in F336W in the ultraviolet have contrasts essentially inverse of each other, with dark spots in the F889N filter being bright in the ultraviolet and bright regions in the F889N filter being dark in the ultraviolet. This is consistent with our interpretation of dark regions in the methane filters as regions with lower clouds, and thus a thicker layer of haze that becomes visible in the ultraviolet. At the eastern end of the perturbed area, a light spot in F889N images, seen faintly as a slightly darker spot in the F336W filter, marks the location of the anticyclone at lower latitudes (~55ºN). The position of this feature is plotted as a blue square in Figure 11a. The most remarkable difference between the images appears in the intermediate region, which in the F336W filter is totally unperturbed, suggesting that the disturbance lies in the upper cloud deck, observed in the FQ937N filter image, without disturbing the hazes above the cloud (West et al., 2009). In this image, the ACA system displays the same morphology as in Figure 6, albeit with lower resolution. A bright spot in the cyclone is suggestive of the clouds visible in Figure 6, and the white collar of both anticyclones can be clearly seen in the lower resolution images. A complete analysis of these images in terms of the vertical cloud structure is undergoing and will be presented elsewhere.

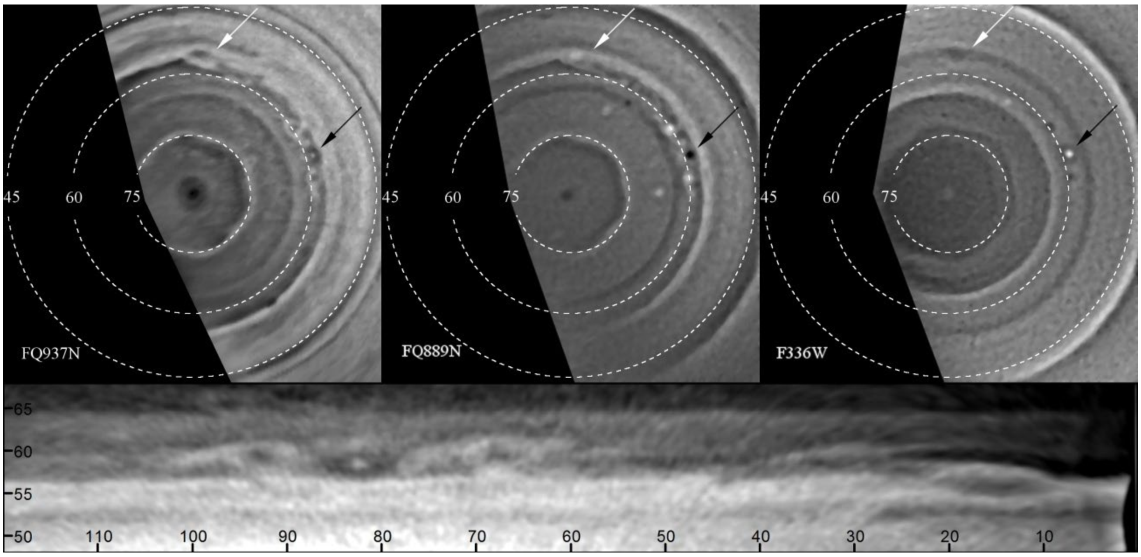

Figure 12. *Polar and cylindrical projections of the polar disturbance.* ***Upper panels:*** *Polar projections of HST WFC3 images of Saturn's North Polar Region taken on 30 June 2015. The WFC3 filter used is indicated in each panel. Black arrows indicate the position of the ACA system and white arrows the vortex at 55ºN.* ***Lower panel:*** *Cylindrical map projection of the FQ937N image covering 20º in latitude and in 120º longitude. The 55ºN vortex is visible at 15º longitude and the ACA system is centered at 83º longitude.*

We measured the positions of cloud features observed in each of the three HST orbits in order to study the zonal motions of features of the ACA system and the disturbed region. Since there are three sets of images, each separated by approximately 20 hours, and the ACA system and most of the disturbed region are covered in all three sets, we have used linear fits to determine the average zonal motion of each individual feature. The results of this analysis in terms of zonal winds are shown in Figure 13. Features pertaining to the disturbance are shown with squares and other features with plus symbols. We observe that the motion of the features in the disturbance follows the average zonal wind profile within the wind measurement errors. This suggests that the disturbed area is the result of the advection of the cloud patterns created by the interaction of the ACA system with the vortex at the south when this eastward moving faster vortex overtook the ACA system, confirming that the perturbation was created by the interaction of the ACA system with the vortex at 55ºN.

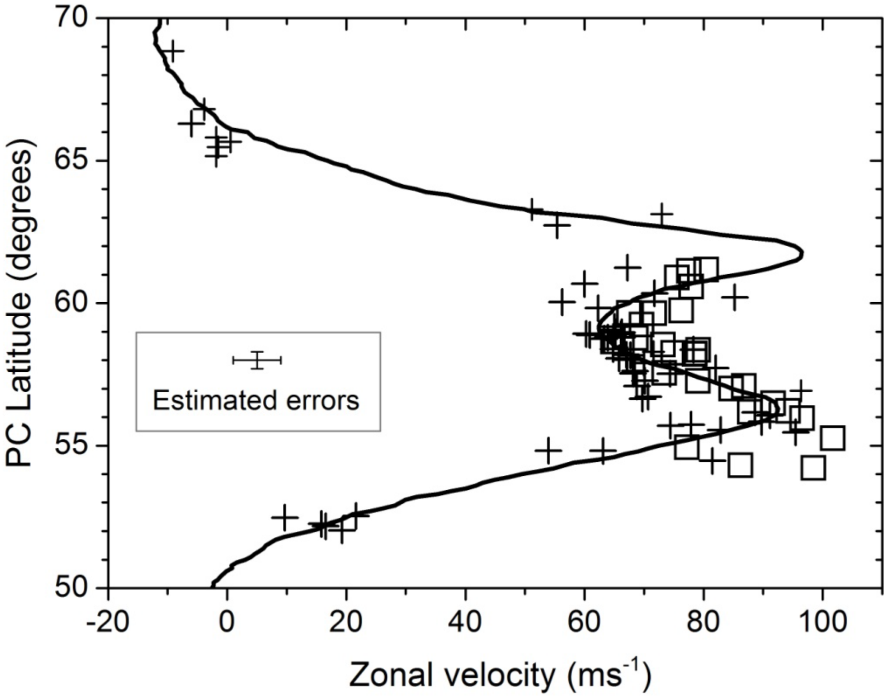

Figure 13. *Velocity measurements determined from cloud tracking in HST images. Squares indicate features pertaining to the disturbance of the ACA system. Plus symbols indicate all other features tracked. Measurements errors are shown in the inset.*

6. Numerical models of the three-vortex system

We performed numerical simulations of the ACA system to establish under what conditions it is stable. We used the Explicit Planetary Isentropic Coordinate model (EPIC) (Dowling et al., 1998) and a one-layer shallow water model (García-Melendo and Sánchez-Lavega, 2017).

The EPIC model is a hydrostatic multilayer model that uses potential temperature as vertical coordinate. In the model, the pressure range for the vertical domain must be specified as well as the number of layers, which determines the vertical resolution. In our study of other regions of Saturn (see e.g. García-Melendo et al., 2007; Legarreta and Sánchez-Lavega, 2008; del Río-Gaztelurrutia et al., 2010), a relatively coarse vertical resolution (8 layers in the 10 mbar to 10 bar pressure range) was sufficient to achieve numerical stability, but this proved not to be the case in the region of the ACA system. With the aid of the much faster one-layer shallow water (SW) simulations, we found that in the region of the ACA the model atmosphere was stable only for layers with depths smaller than ~1000 m (corresponding to barotropic Rossby radius of deformation $L_D = \sqrt{gH}/f \sim 300$ km, $L_D = \sqrt{gH}/f \sim 300$ km, where g = 8.8 m s^{-1} is the gravity acceleration, $H \cong 1000$ m the depth of the layer, and $f \sim 3\times10^{-4}$ s^{-1} the Coriolis parameter). This is consistent with the idea that a small barotropic radius of deformation makes the model atmosphere more stable, because it limits the characteristic size of growing instabilities. Since EPIC is also a multilayer hydrostatic model, the numerical results of the SW model also suggested that the vertical resolution in the EPIC model had to be much higher than in our previous works. To increase vertical resolution without a substantial increase of computational time, we restricted our EPIC-model calculations to a narrower vertical range, between 200 mbar and 500 mbar, to make sure that the top cloud level was included in the model, and the vertical domain was divided in 5 layers.

Morales-Juberías et al. (2010) used EPIC to study the mergers between the spots of the South-South Temperate Zone (SSTZ) of Jupiter. Their results indicate that the vortices on the SSTZ where less prone to merge for high values of the vertical static stability. The coexistence of local convective storms and vortices suggest that the actual value of the static stability in Saturn's upper cloud deck can vary significantly in relatively short distances (Garcia-Melendo et al., 2007), and thus, in our EPIC model, and over the entire simulation domain, we assumed a simple vertical structure with a ~~high~~ constant static stability with Brunt-Väisälä frequency $N^2 = 0.6\times10^{-4}\mathrm{s}^{-2}$ .The exploration of lower values, down to $N^2 = 0.1\times10^{-4}\mathrm{s}^{-2}$ did not lead to substantial differences. On the other hand, the use of the thermal wind equation from CASSINI/CIRS data shows that, at high latitudes, the vertical shear is negligible between 200 mbar and 500 mbar. (García-Melendo et al. 2011). Therefore, we used the zonal wind of García-Melendo et al. (2011) with no vertical shear. Under such conditions, the baroclinic Rossby deformation radius estimated from the vertical static stability of the model atmosphere is $L_D = NH/f \sim 2{,}300$ km, similar to the size of the vortices.

Our simulations were run in a channel 60 degree-long between the planetographic latitudes of 57ºN and 72ºN, (corresponding to planetocentric latitudes from 51.2ºN to 68.1ºN) at a grid resolution of 0.12 degrees grid^{-1}. Boundary conditions in the EPIC model were full slip conditions for the limiting latitudes of the channel, periodic boundary conditions for limiting longitudes, and no heat transfer in the limiting vertical boundaries (Dowling et al., 1998). Vortices were introduced as Gaussian-shaped, geostrophically balanced perturbations in the Montgomery potential field. All the vortices had a zonal length of 3.5°, a meridional extent of 1.5° and tangential velocity at periphery of 50 ms^{-1} It is generally agreed (Legarreta and Sánchez-Lavega, 2008) that vortices in Jupiter and Saturn are thin relative to their horizontal size and to the thickness of the deep atmosphere, with vertical spans between 2 and 4 scale heights. In our case, computational constraints limited our vertical domain to ~1 scale-height, and therefore in our simulations the vortices extended through the whole vertical domain. ~~In the vertical, they extended about two scale-heights (~ 80 km).~~

The zonal wind domain where the vortices live is very narrow, with cyclonic and anticyclonic bands ~2.5º wide. There is therefore little margin to fit vortices at different latitudes if their sizes are comparable to the size of the vorticity domains where they sit (see inset in Figure 1). The best latitudes to reproduce a stable ACA system are 58º for the center of the cyclone and 60º for the centers of the anticyclones, very similar to the measured values for the real vortices. At these latitudes, the three-vortex configuration remained stable for at least 100 days. For other latitudes, it was not possible to adjust drift velocities for the vortices to obtain a compact stable system for such a long time span, or the vortices themselves were not stable as they protruded too deeply into regions of opposite vorticity. Figure 14 shows potential vorticity maps of the ACA system after 15 and 95 days respectively of simulation time.

In addition to constraining the parameters of the EPIC simulations, shallow water models simulated the interaction between the cyclone and the anticyclones as a relative oscillatory movement of the cyclone with respect to the anticyclones (Figure 15), hints of which can be noticed in Figure 5. This behavior reproduces the well-known result that vortices embedded in a sheared background zonal flow with opposite vorticity repel when they come close enough (Youssef and Marcus, 2003.)

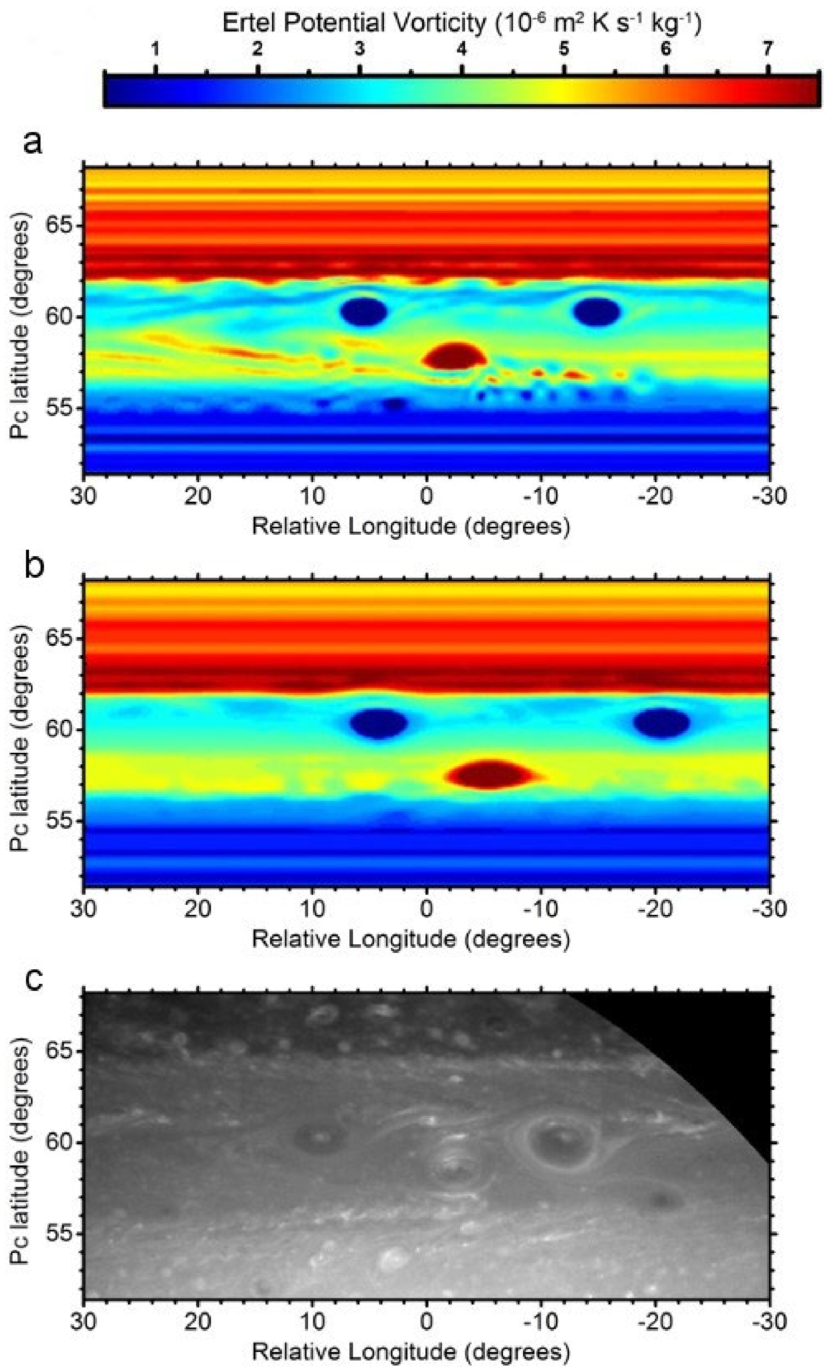

Figure 14. *Ertel potential vorticity maps at the 340 mbar level after EPIC simulations of the ACA system after 10 days (A), and 100 days (B). Panel C shows the ACA system on 27 Feb 2013 for comparison.*

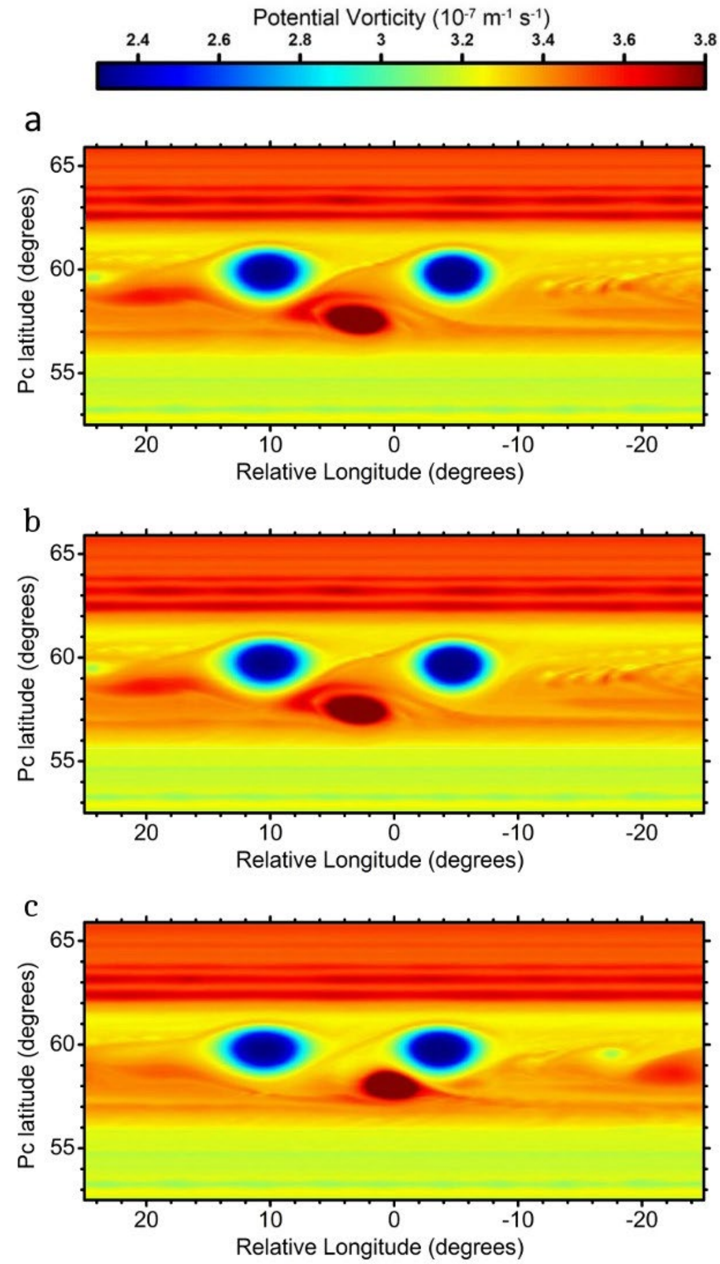

Figure 15*. Potential vorticity maps of shallow water simulations showing oscillations of the cyclonic vortex between the anticyclones for (A) 20 days, (B) 30 days, and (C) 45 days simulation times. The model consisted in a channel with a Rossby radius of deformation of ~300 km. Resolution was of 0.25 degrees pixel^{-1}.*

The mechanism for the long stability and robustness of the ACA system remains unclear. Youssef and Marcus (2003), in their analysis of the Jovian white ovals merger, found that an ACA system of stable vortices could be maintained by a Rossby wave formed in a region of sharp gradient of background potential vorticity, with the anticyclones trapped in the troughs of the wave. They argued that the Jovian white ovals merger and end of the Jovian ACA system occurred due to “hops” of the cyclone and one anticyclone, possible if the approach velocity of the two vortices is sufficiently large to overcome the repulsion. Sanchez-Lavega et al. (2001) argued that the encounter and interaction of the Great Red Spot (northward of the system) and the Jovian ACA (first BC-C-DE, then BE-C-FA, to form finally BA), displaced in latitude the central cyclone favoring the two anticyclone merger. In the case of the Saturnian ACA system, the vortices are embedded in a similar vorticity background, although the jet configuration is different (Figure 4). In our simulation experiments, no clear Rossby wave trap was formed in the potential vorticity field, as anticyclones always drifted away from each other in long-term simulations. We propose that the passage of the large anticyclone located south of the ACA system, which could resemble the interaction of the GRS with the white ovals, because of the different jet structure instead of displacing the cyclone, triggered a disturbance. A detailed study on this complex "four-vortex interaction" is under development and will be presented elsewhere.

7. Summary and conclusions

In this paper, we have described a singular long-lived vortex system in the northern subpolar latitudes of Saturn and a disturbance surrounding this region that developed in mid May 2015. Our main conclusions are:

- We have characterized a triple vortex system formed by a cyclone and two anticyclones, here nicknamed ACA. This system is unique in Saturn and is located in the double-peaked eastward jet at 56º-62ºN planetocentric latitudes. The singular structure of the jet, with two very close regions of opposite vorticities moving at a fast velocity seems to favor the stability of this triple structure. This could be due to the beta effect (Holton, 2004; Sayanagi et al., 2013), that favors a drift to the north for the cyclone and to the south for the anticyclones.

- The ACA system has been tracked unambiguously since 2012, and it is still present in images of Saturn at the time of this writing. The system shows a stable motion consistent with the wind profile, with oscillations of ~10º relative to its average motion with a period of ~4 months.

- Vortices in Saturn can be long lived, surviving for periods of several years. Here, we have demonstrated the survival of a cyclone and its surrounding anticyclones for at least four years, confirming our results of a previous paper in which we found the survival of a similar vortex in the Southern Hemisphere of the planet (del Río-Gaztelurrutia et al., 2010). It is quite likely that the lifetime of the cyclone at the ACA system is even longer, but we have not been able to confirm unequivocally that the single cyclonic vortex detected at ~58ºN from 2009 to 2012 is the same cyclone that forms part of the ACA system.

- We have confirmed the cyclonic and anticyclonic vorticities of these vortices by tracking small clouds motions. The relative vorticity of the cyclone is enhanced to a total value of $\sim 4.5\times10^{-5}\,\mathrm{s}^{-1}$, approximately three times the ambient vorticity due to the jet structure. The total relative vorticity of the anticyclones is $\sim 7\times10^{-5}\,\mathrm{s}^{-1}$ and $\sim 5\times10^{-5}\,\mathrm{s}^{-1}$, 2-3 times the ambient vorticity of the region.

- We have analyzed a disturbance that was detected from ground-based telescopes in mid-May 2015. This disturbance is related to the interaction of the ACA system with a large anticyclonic vortex at lower latitudes (55ºN), moving faster than the ACA system and thus overtaking it. We have tracked the motion of this vortex in the reference system of the ACA, which allows unmistakable detection of the three-vortex system despite the very fast motion of the vortices and the scarcity of data with long time gaps. We have shown that the growth of the disturbance followed the motion of the vortex once it overtook the ACA system. Our tracking of the vortex at

55° further confirms that lifetime of vortices in Saturn can be significantly larger than a year.

- HST images have enabled us to study the local motions at the time of the polar disturbance formed by the interactions of these vortices. The analysis reveals that, in spite of the large morphological changes associated with the disturbance, the features in the region move consistently with the average zonal wind profile. This shows that the clouds created by the interaction or the ACA system with the vortex at its south were essentially advected by the local winds creating a perturbed region without the need for introducing further dynamical mechanisms such as local convection.

- In a numerical model, a stable three-vortex system can be reproduced for a ~100 day time span only when vortices are simulated at the same latitudes as those measured for the real vortices, but it is still unclear what mechanism makes the ACA system a compact stable structure.

Acknowledgements

This work was supported by the Spanish MICIIN projects AYA2015-65041-P (MINECO/FEDER, UE), Grupos Gobierno Vasco IT-765-13, and UFI11/55 from UPV/EHU. EGM is supported by the Serra Hunter Programme, Generalitat de Catalunya. A. Simon, K. Sayanagi and M.H. Wong were supported by a NASA Cassini Data Analysis grant (NNX15AD33G and NNX15AD34G). We acknowledge the three orbits assigned by the Director Discretionary time from HST for this research (DD Program 14064, IP A. Sánchez-Lavega). We are very grateful to amateur astronomers contributing with their images to open databases such as PVOL (http://pvol2.ehu.eus/) and ALPO-Japan (http://alpo-j.asahikawa-med.ac.jp/).

References

Archinal, B.A., A'Hearn, M.F., Bowell, E., Conrad, A., Consolmagno, G.J., Courtin, R., Fukushima, T., Hestroffer, D., Hilton, J.L., Krasinsky, G.A., Neumann, G., Oberst, J., Seidelmann, P.K., Stooke, P., Tholen, D.J., Thomas, P.C., Williams, I.P., 2011. Report of the IAU/IAG working group on cartographic coordinates and rotational elements: 2009. Celestial Mech. Dyn. Astron. 109, 101-135.

Asay-Davis, X.S., Marcus, P. S., Wong, M.H., de Pater, I., 2009. Jupiter's shrinking Great Red Spot and steady Oval BA: Velocity measurements with the 'Advection Corrected Correlation Image Velocimetry' automated cloud-tracking method. Icarus 203, 164-188. doi:10.1016/j.icarus.2009.05.001.

Baines K.H., Delitsky, M.L., Momary., T.W., Brown, R.H. Robert H., Buratti, B.J., Clark, R.N., Nicholson, P.D., 2009. Storm clouds on Saturn: Lightning-induced chemistry and associated materials consistent with Cassini/VIMS spectra. Planet. Space Sci. 57, 1650-1658. doi:10.1016/j.pss.2009.06.025.

Del Genio, A.D., Achterberg, R.K., Baines, K.H., Flasar, F.M., Read, P.L., Sánchez-Lavega, A. Showman, A.P., 2009. Saturn Atmospheric Structure and Dynamics. Chapter 6 in: Saturn from Cassini-Huygens. M. Dougherty, L. Esposito and T. Krimigis (edt.), Springer-Verlag, 113-159.

Dowling, T.E., Fischer, A.S., Gierasch, P.J., Harrington, J., LeBeau, R.P. Jr., Santori, C.M., 1998. The explicit planetary isentropic-coordinate (EPIC) atmospheric model. Icarus 132, 221-238. doi:10.1006/icar.1998.5917.

Dyudina, U.A., Ingersoll, A.P., Ewald, S.P., Porco, C.C., Fischer, G., Kurth, W., Desch, M., Del Genio, A., Barbara, J., Ferrier J., 2007. Lightning storms on Saturn observed by Cassini ISS and RPWS during 2004-2006. Icarus 190, 545-555, doi:10.1016/j.icarus.2007.03.035.

García-Melendo, E., Sánchez-Lavega, A, 2001. A Study of the Stability of Jovian Zonal Winds from HST Images: 1995-2000. Icarus 152, 316-330. doi:10.1006/icar.2001.6646.

García-Melendo, E., Sánchez-Lavega, A., Hueso, R., 2007. Numerical models of Saturn's long-lived anticyclones. Icarus 191, 665-677. doi: 10.1016/j.icarus.2007.05.020.

García-Melendo, E., Pérez-Hoyos, S., Sánchez-Lavega, Hueso, R., 2011. Saturn's zonal wind profile in 2004-2009 from Cassini ISS images and its long-term variability. Icarus 215, 62-74. doi: 10.1016/j.icarus.2011.07.005.

García-Melendo, E., Sánchez-Lavega, A., 2017. Shallow water simulations of Saturn's giant storms at different latitudes. Icarus 286, 241-260. doi: 10.1016/j.icarus.2016.10.006.

Holton, J. R. (2004). An Introduction to Dynamic Meteorology, 4th ed., Academic Press, San Diego, California.

Hueso, R., Legarreta, J., García-Melendo, E., Sánchez-Lavega, A., Pérez-Hoyos, S., 2009. The Jovian anticyclone BA: II. Circulation and interaction with the zonal jets. Icarus 203, 499–515. doi: 10.1016/j.icarus.2009.05.004.

Hueso, R., Legarreta, J., Perez-Hoyos, S., Rojas, J.F., Sanchez-Lavega, A., Morgado, A., 2010a. The international outer planets watch atmospheres node database of giant-planet images. Planet. Space Sci. 58, 1152-1159. doi:10.1016/j.pss.2010.04.006.

Hueso, R., Legarreta, J., Rojas, J.F., Pérez-Hoyos, S., del Río-Gaztelurrutia, T., Sánchez-Lavega, A., 2010b. The Planetary Laboratory for Image Analysis (PLIA). Adv. Space Res. 6, 1120-1138. doi: 10.1016/j.asr.2010.05.016.

Hueso R., Juaristi, J., Legarreta, J., Sánchez-Lavega, A., Rojas, J. F., Erard, S., Cecconi, B., Pierre Le Sidaner, 2017. The Planetary Virtual Observatory and Laboratory (PVOL) and its integration into the Virtual European Solar and Planetary Access (VESPA). Planet. Space Sci. (in the press), doi:10.1016/j.pss.2017.03.014.

Ingersoll, A.P., Beebe, R. F., Conrath, B.J., Hunt, G.E., 1984. Structure and dynamics of Saturn's atmosphere, in *Saturn*, T. Gehrels and M. S. Matthews (eds.), University of Arizona press, Tucson, 195 – 238.

Ingersoll A.P., Dowling, T.E., Gierasch, P.J., Orton, G.S., Read, P.L., Sanchez-Lavega, A., Showman, A.P., Simon-Miller, A.A., Vasavada A.R.., 2004. Dynamics of Jupiter's Atmosphere. Chp. 6 in *Jupiter: The Planet, Satellites & Magnetosphere* (Bagenal, F., McKinnon, W., Dowling T., Editors), Cambridge University Press, pp 105-128.

Legarreta J.J., Sánchez-Lavega, A., 2008. Vertical structure of Jupiter's troposphere from nonlinear simulations of long-lived vortices. Icarus 194, 184-201. doi: 10.1016/j.icarus.2008.02.018.

Li, L., Ingersoll, A.P., Vasavada, A.R., Porco, C.C., Del Genio, A.D., Ewald, S.P., 2004. Life cycles of spots on Jupiter from Cassini images. Icarus 172, 9-23. doi: 10.1016/j.icarus.2003.10.015.

Lii, P.S., Wong, M.H., de Pater, I., 2010. Temporal variation of the tropospheric cloud and haze in the Jovian equatorial zone. Icarus 209, 591-601. doi: 10.1016/j.icarus.2010.05.021.

Marcus, P.S., X. Asay-Davis, M.H. Wong, de Pater, I., 2013. Jupiter's New Red Oval: Dynamics, Color, and Relationship to Jovian Climate Change. Journal of Heat Transfer 135, 011007-1 to 011007-9. doi:10.1115/1.4007666.

Morales-Juberías, R, Brindle, E.S., Dowling, T.E., 2010. Jupiter's South South Temperate Zone vortices: Observations and simulations. Icarus 206, 747-754. doi: 10.1016/j.icarus.2009.10.002.

Mousis, O., and 59 coauthors, 2014. Instrumental Methods for Professional and Amateur Collaborations in Planetary Astronomy. Experimental Astronomy 38, 91-191. doi: 10.1007/s10686-014-9379-0.

de Pater, I., Wong, M. H., Marcus, P.S., Luszcz-Cook, S., Ádámkovics, M., Conrad, A., Asay-Davis, X., Go, C., 2010 Persistent Rings in and around Jupiter's Anticyclones - Observations and Theory. Icarus 210, 742-762. doi: 10.1016/j.icarus.2010.07.027.

Porco, C.C., West, R.A., McEwen, A., Del Genio, A.D., Ingersoll, A. P., Thomas, P., Squyres, S., Dones, L., Murray, C.D., Johnson, T.V., Burns, J. A., Brahic, A., Neukum, G., Veverka, J., Barbara, J.M., Denk, T., Evans, M., Ferrier, J.J., Geissler, P., Helfenstein, P., Roatsch, T., Throop, H., Tiscareno, M., Vasavada, A.R. 2003. Cassini imaging of Jupiter's atmosphere, Satellites and Rings. Science 299 (5612), 1541-1547. doi: 10.1126/science.1079462.

Porco, C.C., West, R.A., Squyres, S., Mcewen, A., Thomas, P., Murray, C.D., Delgenio, A., Ingersoll, A.P., Johnson, T.V., Neukum, G. J. Veverka., Dones, L., Brahic, A., Burns, J.A., Haemmerle, V., Knowles, B., Dawson, D., Roatsch, T., Beurle, K., Owen, W. (2004). Cassini imaging science: Instrument characteristics and anticipated scientific investigations at Saturn. Space Sci. Rev. 115, 363–497. doi: 10.1007/s11214-004-1456-7.

del Río-Gaztelurrutia, T., Legarreta, J., Hueso, R., Pérez-Hoyos, S., Sánchez-Lavega, A., 2010. A long-lived cyclone in Saturn's atmosphere: observations and models. Icarus 209, 665-681. doi: 10.1016/j.icarus.2010.04.002.

Rogers, J.H. (1995) "The Giant Planet Jupiter" Cambridge University Press

Sánchez-Lavega, A., Lecacheux, J., Colas, F., Laques, P., 1993. Ground-Based observations of Saturn's North Polar Spot and Hexagon. Science 260, 329-332. doi: 10.1126/science.260.5106.329.

Sánchez Lavega,A., Rojas, J. F., Acarreta, J. R., Lecacheux, J., Colas, F., Sada, P.V., 1997. New Observations and studies of Saturn's long-lived North Polar Spot. Icarus 128, 322-334. doi: 10.1006/icar.1997.5761.

Sánchez Lavega, A., Rojas, J.F., Hueso, R., Lecacheux, J., Colas, F., Acarreta, J.R., Miyazaki, I., Parker, D.C., 1999. Interaction of Jovian White Ovals BC and DE in 1998 from Earth-Based Observations in the visual range, Icarus 142, 116 – 124. doi: 10.1006/icar.1999.6197.

Sánchez-Lavega, A., Rojas, J.F., Sada, P.V., 2000. Saturn's zonal winds at cloud level. Icarus 147, 405-420. doi: 10.1006/icar.2000.6449.

Sánchez-Lavega, A., Orton, G.S., Morales, R., Lecacheux, J., Colas, F., Fisher, B., Fukumura-Sawada, P., Golisch, W., Griep, D., Kaminski, C., Baines, K., Rages, K., West, R., 2001. The merger of two giant anticyclones in the atmosphere of Jupiter. Icarus 149, 491-495. doi:10.1006/icar.2000.6548.

Sánchez-Lavega A., Pérez-Hoyos, S., Rojas, J. F., Hueso, R., French R. G., 2003. A strong decrease in Saturn's equatorial jet at cloud level. Nature 423, 623-625. doi:10.1038/nature01653.

Sánchez-Lavega A., Hueso, R., Pérez-Hoyos, S., Rojas, J. F., French. R. G., 2004. Saturn's Cloud Morphology and Zonal Winds before the Cassini Encounter. Icarus 170, 519-523. doi: 10.1016/j.icarus.2004.05.002.

Sánchez-Lavega, A., 2005. How long is the day on Saturn? Science 307, 1223–1224. doi:10.1126/science.1104956.

Sánchez-Lavega A., del Río-Gaztelurrutia, T., Delcroix, M., Legarreta, J.J., Gómez-Forrellad, J. M., Hueso, R., García-Melendo, E., Pérez-Hoyos, S., Barrado-Navascués, D., Lillo J., 2012. Ground-based Observations of the Long-term Evolution and Dead of Saturn's 2010 Great White Spot. Icarus 220, 561-576. doi:10.1016/j.icarus.2012.05.033.

Sanchez-Lavega, A., García-Melendo, E., Perez-Hoyos, S., Hueso, R., Wong, M. H., Simon, A. A., Sanz-Requena, J. F., Antuñano, A., Barrado-Izagirre, N., Garate-Lopez, I., Rojas, J. F., del Rio Gaztelurrutia, T., Gómez-Forrellad, J. M., de Pater, I., Li, L. Barry, T. and PVOL contributors, 2016. An Enduring rapidly moving storm as a guide to Saturn's equatorial jet complex structure. Nature Communications 7: 13262. doi: 10.1038/ncomms13262.

Sayanagi, K.M., Dyudina, U.A., Ewald, S.P., Fischer, G., Ingersoll, A.P., Kurth, W. S., Muro, G.D., Porco, C.C., West, R.A., 2013 Dynamics of Saturn's great storm of 2010-2011 from Cassini ISS and RPWS. Icarus 223, 460-478. doi:10.1016/j.icarus.2012.12.013.

Sayanagi, K.M., Dyudina, U.A., Ewald, S.P., Muro, G.D., Ingersoll, A.P., 2014. Cassini ISS observation of Saturn's String of Pearls. Icarus 229, 170-180. doi: 10.1016/j.icarus.2013.10.032.

Simon, A.A., Beebe, R.F., 1996. Jovian Tropospheric Features—Wind Field, Morphology, and Motion of Long-Lived Systems. Icarus 121, 319-330. doi: 10.1006/icar.1996.0090.

Simon, A.A., Wong, M.H., Rogers, J.H., Orton, G.S., de Pater, I., Asay-Davis, X., Carlson, R.W., Marcus, P.S., 2014. Dramatic change in Jupiter's Great Red Spot from spacecraft observations. Astrophysical Journal Letters 797, L31-L34. doi:10.1088/2041-8205/797/2/L31.

Simon, A. A., Wong, M. H., Orton, G. S., 2015. First results from the Hubble OPAL Program: Jupiter in 2015. The Astrophysical Journal 815:55, 8 pp. doi:10.1088/0004-637X/812/1/55.

Smith, B.A, and 25 co-authors, 1981. Encounter with Saturn: Voyager 1 imaging results. Science 212, pp.163-191. doi: 10.1126/science.212.4491.163.

Smith, B.A, and 28 co-authors, 1982. A new look at the Saturn system: The Voyager 2 images. Science 215, pp.505-537. doi:10.1126/science.215.4532.504.

Snyder, J. P., 1987. Map Projections-A Working Manual. U. S. Geological Survey Professional Paper 1395. U. S. Government Printing Office, Washington, DC, 191-202.

Trammell, H.J., Li, L., Jiang, X., Smith, M., Hörst, S. and Vasavada, A., 2014. The global vortex analysis of Jupiter and Saturn based on Cassini Imaging Science Subsystem. Icarus 242, 122-129. doi:10.1016/j.icarus.2014.07.019.

Trammell, H.J., Li, L., Jiang, X., Pan, Y., Smith, M. A., Bering, E. A., Hörst, S. M., Vasavada, A. R., Ingersoll, A. P., Janssen, M. A., West, R. A., Porco, C. C., Li, C., Simon, A. A., and Baines, K. H., 2016. Vortices in Saturn's Northern Hemisphere (2008–2015) observed by Cassini ISS. J. Geophys. Res. Planets 121, 1814–1826, doi:10.1002/2016JE005122.

Vasavada, A.W., Hörst, S.M., Kennedy, M.R., Ingersoll, A.P., Porco, C.C., Del Genio, A.D., West, R.A., 2006. Cassini imaging of Saturn: Southern hemisphere winds and vortices. Journal of Geophysical Research, 111, E05004. doi:10.1029/2005JE002563.

West, R.A., Baines, K.H., Karkoschka, E., Sánchez-Lavega, A., 2009. Clouds and aerosols in Saturn's atmosphere. In: Dougherty, M.K., Esposito, L.W., Krimigis, S.M. (Eds.), Saturn from Cassini-Huygens. Springer, Netherlands, pp.161–179.

Wong, M.H., de Pater, I., Marcus, P.S., Asay-Davis, X., Go, C.Y., 2011. Vertical structure of Jupiter's Oval BA before and after it reddened: What changed? Icarus 215, 211-225. Doi:10.1016/j.icarus.2011.06.032.

Youssef, A. and Marcus, P. S., 2003. The dynamics of Jovian white ovals from formation to merger. Icarus 162, 74-93. doi: 10.1016/S0019-1035(02)00060-X.